JOURNAL OF COMPUTATIONAL PHYSICS 103, 300–319 (1992)

Computational Implementation of a Coupled Plasma–Neutral Fluid Model

E. L. VOLD,* F. NAJMABADI, AND R. W. CONN

Institute of Plasma and Fusion Research, Department of Mechanical, Aerospace, and Nuclear Engineering, University of California, Los Angeles, Los Angeles, California 90024-1597

Received October 30, 1990; revised October 17, 1991

This paper describes the computational transport of coupled plasma–neutral fluids in the edge region of a toroidally symmetric magnetic confinement device, with applications to the tokamak. The model couples neutral density in a diffusion approximation with a set of transport equations for the plasma including density, classical plasma parallel velocity, anomalous cross-field velocity, and ion and electron temperature equations. The plasma potential, gradient electric fields, drift velocity, and net poloidal velocity are computed as dependent quantities under the assumption of ambipolarity. The implementation is flexible to permit extension in the future to a fully coupled set of non-ambipolar momentum equations. The computational method incorporates sonic flow and particle recycling of ions and neutrals at the vessel boundary. A numerically generated orthogonal grid conforms to the poloidal magnetic flux surfaces. Power law differencing based on the SIMPLE relaxation method is modified to accomodate the compressible reactive plasma flow with a "semi-implicit" diffusion method. Residual corrections are applied to obtain a valid convergence to the steady state solution. Results are presented for a representative divertor tokamak in a high recycling regime, showing strongly peaked neutral and plasma densities near the divertor target. Solutions show large poloidal and radial gradients in the plasma density, potential, and temperatures. These findings may help to understand the strong turbulence experimentally observed in the plasma edge region of the tokamak.

I. INTRODUCTION

A controlled fusion power reactor requires plasma at very high temperatures ($\sim 10^8$ K) which cannot be contained in known materials. One solution is to use magnetic confinement in which the Lorentz force acts on the plasma charged particles, constraining them to follow the magnetic field lines. The magnetic topology generated in the tokamak device provides a closed path for the plasma in the shape of a torus.

The plasma diffuses across the magnetic field lines in a poorly understood "anomalous" transport process to the vessel walls. This creates a wide range of plasma–surface interactions which dominate the physics in the tokamak "plasma edge" region, or scrape off layer (SOL), where the magnetic field lines terminate on the vessel wall. The plasma flows to the vessel walls and is neutralized upon contact. The neutral particles are reflected and transported through the plasma until re-ionized by electron impact ionization. The re-ionized plasma streams to the wall and is again reneutralized in a "recycling" process until the neutral particles escape the plasma into a pumping duct and are gettered from the system. Understanding this recycling is vital to understanding the global magnetic confinement of the plasma and to design the particle and heat exhaust systems for steady state operation.

The plasma edge region can be assumed toroidally symmetric in many tokamak devices, but the edge physics drives strong radial and poloidal gradients which necessitates a two-dimensional (2D) modelling capability in the tokamak edge plasma region. Magnetic divertors often have significant recycling zones in front of the target, which allows a significant temperature gradient along the field line in the divertor. Poloidally varying radial profiles of the plasma parameters throughout the recycling zone necessitate a self-consistent plasma–neutral calculation to predict the two-dimensional profiles and plasma behavior in the divertor recycling zone.

Reviews of edge physics issues are given in Refs. [1–4]. A detailed review of edge plasma modeling including impurity transport is presented by Post and Lackner [5]. Harrison *et al.* [6] present a divertor design review with analytical fits for useful plasma–surface interaction data.

Several groups have reported two-dimensional (2D) steady state results in the plasma edge region [7–20]. A summary of the 2D codes was given in Vold [7]. The equations solved vary in format but are all variations on the plasma fluid equations of Braginskii [21]. A classical parallel momentum equation is solved, and energy equations are solved for one (T) or two (T_i and T_e) temperatures. The radial transport is assumed to be an anomalous flux and generally diffusive.

The drift flows have been neglected until recent work [7,

* Present address: Applied Theoretical Physics Division, Los Alamos National Laboratory, X-4, MS F664, Los Alamos, NM 87545.

0021-9991/92 $5.00

9, 10, 19, 20], where attempts at self-consistent drifts have begun. Gerhauser and Claassen developed a fluid model with equilibrium plasma currents in a "semi-self-consistent approximation" to study the poloidal drift rotation of a limiter plasma [10]. Recently, they improved the model to include a more self-consistently calculated current and electric field and applied the model to explain poloidal asymmetries observed experimentally on the TEXTOR tokamak edge plasma [9]. On D-III, the influence of poloidal drift flow on ambipolar electric potential has been reported [19]. Two groups [7, 13] have included parallel electric field terms which drive a classical radial drift. This term has been discussed by Hinton *et al.* [22] in relation to the H-mode trigger mechanism.

Neutral transport models incorporate either simple analytic approximations (e.g., [12]) or involve iterating for the steady state solution with a Monte Carlo (MC) treatment for the neutral transport (e.g., [16, 17]). The first approach is not intended for time dependent resolution of the physics. It does not allow the neutrals to evolve as a separate species, nor can appropriate boundary conditions for the neutrals be readily applied. The second approach, using MC codes, is very costly in computer time and impractical for time dependent problems. It is difficult to couple a finite differenced plasma solution to a statistical (Monte Carlo) neutral solution on the same computational grid and to assure convergence. An alternative approach is to use a diffusion approximation for the neutrals to allow the self-consistent coupling of the discretized equations for both the plasma and the neutral fluids. This approach is described in this report and treated in greater detail elsewhere [7, 23].

Only steady state results have been reported with one exception [7]. Three groups [7, 11, 18] formulate the problem in general orthogonal co-ordinate systems, two groups use toroidal metric co-ordinates [9, 13] while others appear to use rectangular geometry. On D-III [18] and on INTOR [16] results are reported in realistic magnetic flux geometry. An approximation to the non-orthogonal target plate orientation with respect to the poloidal field lines has been reported [7] using the code described in this report.

Solution methods vary and three authors have detailed their solution method [7, 10, 12]. Braams [12] solves the plasma equations using a relaxation scheme similar to that used in the present study with implicit differencing for the advanced time step. The coupled algebraic equations are solved with a modified Strongly Implicit Procedure [24]. Gerhauser and Claassen use a modified version of the McCormack method [25]. A less specific numerical "splitting technique," possibly variations of the ADI (alternating-direction-implicit) method, is also reported in [13, 15] as are variations of the PIC (particle-in-cell) method in [18], and a Newton–Raphson block iteration scheme in [20].

Following a brief survey of plasma edge modelling, a 2D computational model is developed in this report which has been implemented in the EPIC (edge plasma implicit computation) code [10]. Magnetic flux surface equilibrium is assumed constant in time. Core effluxes to the plasma edge region are prescribed as functions of time to simulate the coupling with an evolving core plasma.

II. GOVERNING EQUATIONS OF THE ANALYTIC MODEL

II.1. *Plasma Equations*

The plasma equations presently used in the EPIC (edge plasma implicit computation) code are derived for the toroidally symmetric case and discussed in references [7, 23, 26] and are summarized here. The equations are solved for the plasma quantities: density, n; parallel velocity, u; radial velocity, v; electron and ion temperatures, T_e and T_i; and the coupled neutral density, n_0. Parallel velocity is determined from the classical momentum equation but the cross-field (radial) flux is assumed anomalous.

The metric used for the transport equations in toroidal geometry is: $H = h_\theta h_r R$, where $R = R(\theta, r)$ is the distance to the toroidal axis, and the metrics, h_θ and h_r, depend on the poloidal magnetic flux surface. The plasma fluid velocity components are: $\mathbf{u} = u\mathbf{s} + v\mathbf{r} + w\mathbf{q}$, where $\mathbf{s}$ is the unit vector parallel to the magnetic axis, $\mathbf{r}$ is in the magnetic surface gradient direction, and $\mathbf{q}$ is the drift direction defined as $\mathbf{q} = \mathbf{r} \times \mathbf{s}$. The relation between the toroidal coordinates: $\boldsymbol{\theta}$, $\mathbf{r}$, $\boldsymbol{\phi}$ and the coordinates aligned with the magnetic field: $\mathbf{s}$, $\mathbf{r}$, $\mathbf{q}$ is shown in Figs. 1 and 2.

Drift velocity, w, is assumed for computational convenience to have a small influence on the plasma density and temperature solution. This is found (as discussed in Section IV and in [7]) to be a reasonable assumption near the target and in the recycling regions, but is poor in the regions near the separatrix/tangency away from the target plate. A self-consistent drift is planned in future computations.

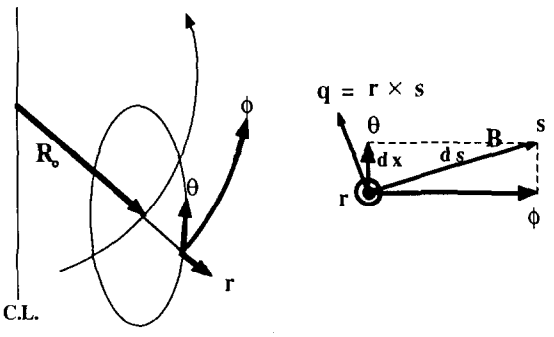

FIG. 1. Coordinate systems: Relationship between the magnetic geometry coordinates: $\mathbf{s}$, $\mathbf{r}$, $\mathbf{q}$, and the toroidal coordinates: $\boldsymbol{\theta}$, $\mathbf{r}$, $\boldsymbol{\phi}$.

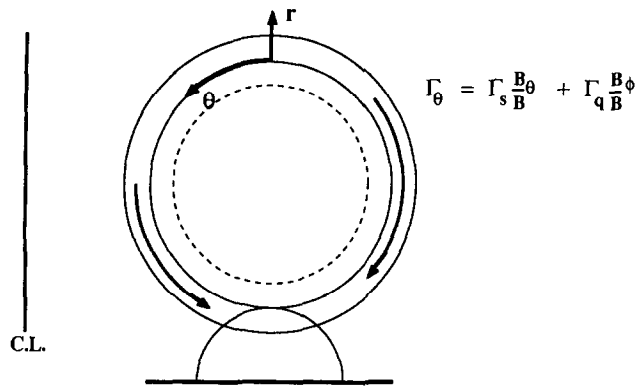

FIG. 2. Poloidal cross section showing poloidal components of flux with contributions from the parallel and drift flux terms. The magnetic field weighting factors for each flux follow directly from Fig. 1.

The following equations can be modified for the assumption that drift velocity is *not* negligible in the coupled equations by replacing the poloidal component of parallel flow, $(B_\theta/B)u$, with the total poloidal flow, u_θ, where $u_\theta = (B_\theta/B)u + (B_\phi/B)w$, and w is the plasma drift velocity. That case requires coupling another momentum equation to the coupled system [7, 26].

The governing plasma equations implemented in the present EPIC code are

Continuity:

$$\frac{\partial n}{\partial t} + \frac{1}{H}\frac{\partial}{\partial \theta}\left(nh_r R \frac{B_\theta}{B} u\right) + \frac{1}{H}\frac{\partial}{\partial r}(nvh_\theta R) = S_n(n_0). \quad (1)$$

Parallel momentum:

$$\frac{\partial(mnu)}{\partial t} + \frac{1}{H}\frac{\partial}{\partial \theta}\left(h_r R\left(mnu\left(\frac{B_\theta}{B}u\right) - \frac{\eta_0}{h_\theta}\left(\frac{B_\theta}{B}\right)^2 \frac{\partial u}{\partial \theta}\right)\right) + \frac{1}{H}\frac{\partial}{\partial r}\left(h_\theta R\left(mnuv - \frac{\eta_{an}}{h_r}\frac{\partial u}{\partial r}\right)\right) + \frac{B_\theta}{Bh_\theta}\frac{\partial p}{\partial \theta} = S_p(n_0)\, s. \quad (2)$$

Radial flux:

$$\begin{aligned}\Gamma_r &= nv_r \\ &= nv_{an} + nv_{\mathrm{cl}} - \frac{D_{an}}{h_r}\frac{\partial n}{\partial r} \\ &= n\left(v_{an} + \frac{B_\phi}{B^2 h_\theta}\frac{0.71}{e}\frac{\partial T_e}{\partial \theta}\right) - \frac{D_{an}}{h_r}\frac{\partial n}{\partial r}. \end{aligned} \quad (3)$$

Ion temperature:

$$\begin{aligned}&\frac{\partial(\frac{3}{2}nT_i)}{\partial t} + \frac{1}{H}\frac{\partial}{\partial \theta}\left(h_r R\left(\frac{3}{2}nT_i\left(\frac{B_\theta}{B}u\right) - \left(\frac{B_\theta^2}{B^2}\frac{\kappa_{i\parallel}}{h_\theta}\right)\frac{\partial T_i}{\partial \theta}\right)\right) \\ &\quad + \frac{1}{H}\frac{\partial}{\partial r}\left(h_\theta R\left(\frac{3}{2}nT_i v - \frac{\kappa_{i-an}}{h_r}\frac{\partial T_i}{\partial r}\right)\right) \\ &\quad + \frac{nT_i}{H}\left(\frac{\partial}{\partial \theta}\left(h_r R\left(\frac{B_\theta}{B}u\right)\right) + \frac{\partial}{\partial r}(h_\theta R v)\right) \\ &= Q_A + S_{Ei}(n_0) - uS_{pi}(n_0)_s - vS_{pi}(n_0)_r \\ &\quad + S_n(n_0)\frac{m}{2}(u^2 + v^2). \end{aligned} \quad (4)$$

Electron temperature:

$$\begin{aligned}&\frac{\partial(\frac{3}{2}nT_e)}{\partial t} + \frac{1}{H}\frac{\partial}{\partial \theta}\left(h_r R\left(\frac{3}{2}nT_e\left(\frac{B_\theta}{B}u\right) - \left(\frac{B_\theta^2}{B^2}\frac{\kappa_{e\parallel}}{h_\theta}\right)\frac{\partial T_e}{\partial \theta}\right)\right) \\ &\quad + \frac{1}{H}\frac{\partial}{\partial r}\left(h_\theta R\left(\frac{3}{2}nT_e v - \frac{\kappa_{e-an}}{h_r}\frac{\partial T_e}{\partial r}\right)\right) \\ &\quad + \frac{nT_e}{H}\left(\frac{\partial}{\partial \theta}\left(h_r R\left(\frac{B_\theta}{B}u\right)\right) + \frac{\partial}{\partial r}(h_\theta R v)\right) \\ &= -Q_A + S_{Ee}(n_0). \end{aligned} \quad (5)$$

In the electron temperature equation it was found necessary to define a flux limited parallel heat conductivity [12, 27, 28] to avoid unrealistically large heat flux between the x-point and the target in some cases, especially during transients [7]. The anomalous transport diffusion coefficient (in Eq. (3)) is a constant chosen from empirical considerations and is generally of the order 1. $m^2\, s^{-1}$.

The dependent ambipolar plasma potential, Φ, is calculated in the SOL by integrating the parallel Ohm's law from the target boundary condition, where the plasma potential is taken to be $3T_e/e$. The poloidal component of the parallel ambipolar Ohm's law is

$$\frac{B_\theta}{Bh_\theta}\frac{\partial}{\partial \theta}\Phi = \frac{B_\theta}{neBh_\theta}\frac{\partial}{\partial \theta}p_e + \frac{0.71}{e}\frac{B_\theta}{Bh_\theta}\frac{\partial}{\partial \theta}Te + dP(n_0)\, s. \quad (6)$$

The drift velocity, w, is calculated from the solution to the radial component of ion momentum:

$$w = -\left(\frac{1}{h_r}\frac{\partial \Phi}{\partial r} + \frac{1}{neh_r}\frac{\partial p_i}{\partial r}\right)\Big/ B. \quad (7)$$

II.2. *Plasma–Neutral Volumetric Source Terms*

The neutral–plasma volumetric source terms in Eqs. (1)–(5), can be written in a simple manner for the two reactions considered here, electron impact ionization and charge exchange. Electron impact ionization produces a net change in the plasma ion species. Charge exchange

contributes to momentum exchange primarily through the ions. Both interactions contribute to the energy exchange terms.

The neutral–plasma source terms can be written for the continuity equation:

$$S_n(n_0) = nn_0\langle\sigma v\rangle_{ei}; \tag{8}$$

for the momentum equation:

$$S_p(n_0) \cong nn_0\langle\sigma v\rangle_{ei} m_0 v_{0d} + nn_0\langle\sigma v\rangle_{cx}(m_0 v_{0d} - m_i u_i); \tag{9}$$

and for the energy/temperature equations:

$$S_{Ti}(n_0) \cong nn_0\langle\sigma v\rangle_{ei} E_0 + nn_0\langle\sigma v\rangle_{cx}\left(\left(E_0 + \frac{m_0 v_{0d}^2}{2}\right) - \left(\frac{3}{2}T_i + \frac{m_i V_i^2}{2}\right)\right) \tag{10}$$

$$S_{Te}(n_0) \cong -nn_0\langle\sigma v\rangle_{ei} E_{ioniz}; \tag{11}$$

where E_0 is the average neutral energy, and v_{0d} is the neutral fluid diffusion velocity, given by the diffusion assumption as, $v_{0d} = -(D_{n_0}/n_0)\nabla n_0$. The neutral diffusion coefficient, D_{n_0}, is described in the following and is equal to: $D_{n_0} \equiv u_0^2/3n\langle\sigma v\rangle_{tot}$. The value $E_{\text{ioniz}} = f(T_e, n)$ is the electron energy loss per ionization.

II.3. *Neutral Diffusion Approximation*

The neutral density, n_0, is evaluated using a neutral diffusion approximation [7, 23] assuming that electron impact ionization is the dominant "absorption" event, and that charge exchange is the "scattering" event. With this analogy, the development follows the conventional diffusion theory (e.g., see Duderstadt and Hamilton [29]).

The continuity equation for neutrals is

$$\frac{\partial n_0}{\partial t} + \nabla\cdot(\Gamma_{n_0}) = -S_n(n_0) = -nn_0\langle\sigma v\rangle_{ei}. \tag{12}$$

The second moment of the neutral transport equation can be simplified to give an expression for the neutral current flux, Γ_{n_0},

$$\Gamma_{n_0} \approx \frac{-\lambda_{tr}}{3}\nabla(n_0 u_0), \tag{13}$$

yielding a "conservative flux form" of the neutral diffusion equation as

$$\frac{\partial n_0}{\partial t} + \nabla\cdot\left(\frac{-\lambda_{tr}}{3}\nabla(n_0 u_0)\right) = -S_n(n_0) = -nn_0\langle\sigma v\rangle_{ei}. \tag{14}$$

The average speed of the neutrals, u_0, is required to evaluate neutral density in Eq. (14). A simple approximation is that the neutrals are in one energy group at the same energy as the average local ion temperature, the one group-ion temperature equilibrium (OGITE) approximation. Thus, u_0 is evaluated from the average Maxwellian ion at temperature, T_i:

$$u_0 = \sqrt{8kT_i/\pi M}. \tag{15}$$

The assumption of one energy group for the neutrals in local thermal equilibrium with the ions is valid for

$$\lambda_{cx} \leqslant L_T \equiv \frac{T_i}{(\partial T_i/\partial x)}. \tag{16}$$

Discussion of this and additional criteria with comparisons of the neutral diffusion results to Monte Carlo transport results are documented elsewhere [7, 23]. It was shown there that consistency with the OGITE assumption implies $\nabla u_0 < \nabla n_0$ and so the neutral flux in Eq. (13), should be approximated:

$$\Gamma_{n_0} \approx \frac{-\lambda_{tr}}{3} u_0 \nabla n_0 \equiv -D_{n_0}\nabla n_0. \tag{17}$$

With these considerations we can write the neutral OGITE diffusion approximation,

$$\frac{\partial n_0}{\partial t} + \nabla\cdot(-D_{n_0}\nabla n_0) = -S_n(n_0) = -nn_0\langle\sigma v\rangle_{ei}, \tag{18}$$

with the neutral diffusion coefficient, D_{n_0} defined as

$$D_{n_0} \equiv \frac{\lambda_{tr}}{3} u_0 \equiv \frac{u_0^2}{3n\langle\sigma v\rangle_{tot}}. \tag{19}$$

An outward directed flux and an inward directed flux, with particle conservation at the boundary, can be combined to yield a generalized Marshak-type boundary condition that is appropriate for the diffusion approximation [30],

$$\frac{(1-\alpha)}{(1+\alpha)}\frac{n_0 u_0}{2} \pm D_{n_0}\nabla n_0 = S_0, \tag{20}$$

where the $\pm$ sign is chosen so that ∇n_0 is outward directed. The source term S_0 is an inward directed source calculated so that total particle conservation is maintained at the boundary and correctly partitioned between plasma and neutral particles. The reflection coefficient for neutrals at the boundary, α, must be determined by some means other than the present code to fix a boundary condition on the neutrals.

It can be evaluated in analytic approximations, taken from empirical data or from Monte Carlo results for boundaries in ducts with complex geometries. The exhaust efficiency characterizing a unique divertor or limiter is equivalent to specifying an α for that divertor or limiter at the plasma–duct boundary. Neutral reflection at the duct is discussed in Section II.4.iii.

In making a one group diffusion approximation for the neutrals, the physics of neutral transport is considerably simplified, especially in grouping the low energy neutral molecules with the neutral atomic species. These issues and a detailed comparison to Monte Carlo results have been reported [7, 23] to justify this approach. The neutral diffusion results were found to be surprisingly accurate (within tens of percent) over a range of typical plasma edge conditions, despite the marginal validity of the criteria given in Eq. (16).

II.4. *Plasma–Neutral Boundary Conditions*

i. *Boundary types.* An example of a SOL geometry using magnetic flux surface metrics is shown in Fig. 3, with the boundary types labelled for reference. These types include:

(A) *The core–SOL boundary.* This can be specified along the limiter tangency, the divertor separatrix, or slightly inside the last closed flux surface. Plasma particle and heat efflux flowing from the core plasma are sources to the SOL plasma. This is the fixed core flux, or "fueling" flux, due to plasma particle feuling and external power inputs such as NBI or ICRF.

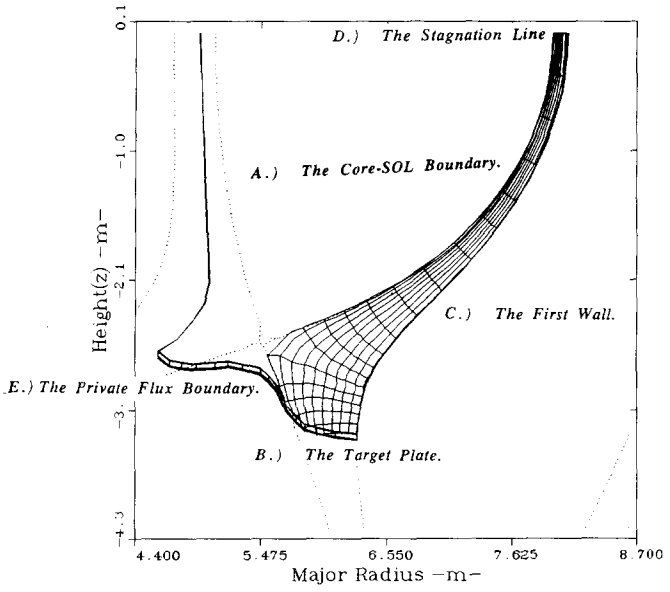

FIG. 3. Example of a computational grid in magnetic flux surface coordinates, with the types of boundary conditions labelled. In this example, the non-orthogonal target inclination is approximated by varying the number of "poloidal" grid cells along different magnetic flux surfaces.

Neutrals which are lost across this boundary from the edge plasma back into the core are re-ionized and must be returned or recycled to the edge region as plasma in a self-consistent calculation. The preferred form of this boundary condition specifies the "fueling" flux and calculates the recycled flux to evolve self-consistently.

(B) *The target plate.* The magnetic field lines in the SOL terminate at a wall or special target plate in the limiter or divertor configuration, where the plasma potential sheath forms, drawing the plasma to this surface at the local plasma sound speed. Upon striking the surface the plasma is neutralized, forming an "exit" from the computational region for the plasma. The particles are returned as neutrals, so the loss of plasma flux equals the neutral source for the particle boundary conditions at the target. The temperature boundary conditions are in the form of a heat flux loss prescribed by sheath theory, as discussed in this section.

(C) *The first wall.* The radial flux of plasma is generally small so that the efflux to the first wall is minimal compared to the loss at the target plate. Flux boundary conditions are used throughout this study with gradient scale lengths set to large values corresponding to a small diffusive flux at this boundary. The plasma loss term is set equal to the neutral source term to account for particle recycling from the first wall. Plasma sheath effects are neglected at the first wall.

A portion of the boundary along the first wall is specified to be a duct for pumping neutrals. This boundary is modelled through a neutral flux reflection coefficient (in Eq. (20)) of less than one.

(D) *The stagnation lines.* In many cases it is convenient to model the SOL from a line which is halfway along the magnetic field connection length in the edge. For a toroidally symmetric device with one poloidal x-point (or limiter) this line will be about halfway around the torus poloidally from the x-point. Assuming flow symmetry the net parallel flow component is zero here and thus the name, "stagnation line." Symmetry again suggests a stagnation flow line exists inside (at a smaller minor radius than) the limiter tangency or x-point for the parallel velocity. Stagnation boundaries are modeled by specifying zero flux, setting the velocities and gradient transported quantities to zero.

(E) *The private flux boundary.* This follows the divertor separatrix line from the x-point to the target. An estimate for the flux across this boundary is derived by relating the cross-field to the parallel transport through the continuity equation. An alternative implementation included in the computational model is to extend the grid beyond the separatrix line to the symmetry line of the device, where zero gradient conditions can be specified.

ii. *Plasma flux at the core–SOL interface.* The particle flux, Γ_{bc}, and heat flux, Q_{bc}, at the core–SOL boundary are not specified independently and must be consistent with the

global confinement times for particles, τ_p, and for energy, τ_E. The flux *BC* can be specified as a function of time to simulate plasma startup conditions and various time dependent characteristics of the core such as a reduced flux at the $L \rightarrow H$ transition, flux "pulses" observed in the ELMs, sawteeth propagation from the core to the edge plasma, and so on.

A self-consistent condition at the core–SOL boundary is the most important and yet elusive requirement for properly solving the edge plasma problem. A core efflux based on fueling or pumping exhaust rate requirements is specified, and a self-consistently calculated neutral flux from the edge–core recycling is added. In this way the total flux from the core to the edge evolves consistently with the pumping requirements, and the value of density and temperature resulting at the edge are consistent with this combined total flux including effects of edge recycling. The fueling rate is based on steady state machine design requirements which are assumed to observe the plasma beta and density limits. As a simplification of the actual conditions in operating experimental devices, the fueling rate is assumed to be independent of the recycling. In lieu of solving transport throughout the complete core and edge coupled plasma regions, the superposition of recycled flux and fueling flux at the separatrix boundary is a reasonable approximation in which some of the problem nonlinearity is treated. This is described in greater detail in Refs. [7, 23].

An effective reflection coefficient for neutrals at this boundary, α_{cs}, resulting from charge exchange in the core plasma is estimated [23] for use in the neutral boundary condition (Eq. (20)). The fraction not reflected, $(1-\alpha_{cs})$, is ionized in the core region and diffuses back to the SOL as plasma with the radial plasma velocity, v. The time dependence of this core-SOL recycling is modelled assuming a "neutral edge region" just inside the last closed flux surface with an average neutral density, n_{0c} (core neutral density), an average density of ions due to the neutral re-ionization, n_{0i}, and a radial thickness equal to a locally determined neutral mean free path for ionization, λ_{n0c}. Integrating equations for these quantities determines the re-ionized neutral flux, $(n_{0i}v)$, which is added to the prescribed flux from the core, $\Gamma_c(t)$ to determine the time-dependent flux boundary condition on the plasma density.

iii. *Neutral reflection at the duct.* The neutral diffusion model does not apply beyond the plasma region. A reflection coefficient, α, equal to the probability of return to the plasma from the duct at the plasma–duct interface must be determined for the neutral density boundary condition (Eq. (20)). The neutral duct reflection coefficient is derived independently from comparison to experiment, from Monte Carlo results, or from an analytic form derived in terms of the capacitance of the pumping duct. On Textor with the ALT-II toroidally symmetric belt limiter, comparisons of experimental data and Monte Carlo simulations [31] show that this probability is typically in the range 0.8–0.9.

iv. *Sheath boundary conditions.* The plasma in the vicinity of a material surface forms a "plasma sheath" regardless of angle of incidence of the magnetic field lines [32]. We follow the usual convention in modelling the edge, that the sheath forms only at the surface which is normal or strongly oblique to the magnetic field lines, which is designated the "target" or "plate" in the limiter or divertor configuration. Cross-field transport losses to the first wall are prescribed fluid fluxes, without the sheath taken into account.

The sheath boundary conditions in edge modeling have been discussed elsewhere [26, 33], and we summarize the applicable results. Plasma fluid (or kinetic) models are applied to evaluate transmission coefficients, δ, which relate plasma density flux, electron energy flux, and ion energy flux through the plasma sheath as a function of the change in plasma potential through the sheath. Setting general flux quantities equal to sheath transmitted quantities, the sheath *BC* becomes

$$\Gamma_n = (n\mathbf{v})_{\text{sheath}} = \delta n C_s \tag{21}$$

$$\Gamma_{Ti} = \left(\left(\frac{5}{2} nT_i + \frac{M}{2} V^2\right) v - \kappa \nabla T_i\right)_{\text{sheath}} = \delta_i n C_s T_i \tag{22}$$

$$\Gamma_{Te} = \left(\left(\frac{5}{2} nT_e\right) v - \kappa \nabla T_e\right)_{\text{sheath}} = \delta_e n C_s T_e. \tag{23}$$

The coefficient of $\frac{5}{2}$ accounts for the total convective flux, compared to $\frac{3}{2}$ used in Eqs. (4) and (5), where the $p\nabla\cdot\mathbf{u}$ contribution is separated to the right-hand side for computational convenience as described in Section III.3.

The density flux transmission coefficient, δ, is set equal to one, corresponding to the Bohm sheath criterion. This establishes the boundary condition on parallel velocity, u:

$$\mathbf{v}_{\text{sheath}} = u = C_s. \tag{24}$$

where C_s is the plasma sound speed. The boundary conditions on temperatures apply to the parallel component of the energy flux where δ_i and δ_e must be specified. There is a range in values for the δ's in the literature [34], where: $\delta_i \approx 1.5$–3.5 and $\delta_e \approx 4.8$–5.5. We follow the standard practice to fix these transmission coefficients as constants in the computations. The default values used here are $\delta_i = 2.5$ and $\delta_e = 5.5$. Results have been seen to be relatively insensitive to the value chosen.

III. COMPUTATIONAL METHODS

III.1. *Computational Requirements of the Plasma Fluid Equations*

In the fluid equations we have coupled the plasma density, the parallel velocity, a radial anomalous velocity, T_i,

and T_e (Eqs. (1)–(5)) with the neutral density in a diffusion approximation (Eqs. (18)–(19)). The neutral transport is purely (elliptic) diffusive while the plasma equations are combined convective–diffusive (parabolic) equations that are typical of ordinary fluid flow except in two important aspects. First, the continuity equation has a reactive volumetric source term due to neutral re-ionization which dominates near the sheath target region and strongly influences the solution through the buildup of density by plasma–neutral recycling. Second, the plasma sheath boundary condition at the target fixes the plasma fluid outflow speed from the region to be sound speed, and thus the exit flow velocity is determined by the plasma temperature. Both these factors are significant departures from conventional non-reactive fluid flow and must be treated appropriately in the computational method.

Plasma velocity is significant in the edge region. It is reasonable to assume that the plasma flow remains subsonic throughout the computational domain, but is sonic at the target boundary. The upstream flow remains at a low speed and thus would be incompressible in a conventional fluid. However, because the plasma density varies spatially, the plasma fluid must be treated numerically as a compressible fluid (Section III.4).

The geometry for a typical divertor problem is shown in Fig. 3, where an orthogonal grid is imposed on the poloidal magnetic flux surfaces. The third dimension of the grid (depth into the page) varies as a function of position to model the toroidal distance for each grid cell. The plasma flows from the core into the SOL and then follows the magnetic flux lines to the target or plate boundary, emphasizing the need for a flexible computational method to deal with arbitrary orthogonal geometry.

The spatial grid requirements are limited by the solution gradients which are steepest near the separatrix or tangency line and are steepest poloidally near the plasma flow exit at the target plate. The radial gradients are established by the balance of parallel and cross-field transport of the plasma. The axial (poloidal) gradients in the plasma parameters are can be limited by the neutral density scale lengths in regimes where recycling is important. The neutral and the plasma transport physics differ, so the neutral density scale lengths are shorter and can limit the plasma scale lengths in the high density, high recycling regimes. A dense grid near the target is needed to resolve the neutral gradients there. A finite difference scheme is necessary which allows variable grid spacing to resolve each of these scales properly.

Time step restrictions are related to the advection of the plasma flow. The limiting time step is determined at the grid cells immediately in front of the target where the plasma flow becomes sonic, discussed further in III.7.

In the literature for fluid computations there are two methods which have been widely used and also successfully applied to the edge plasma. These are the MacCormack method [25, 35] developed in the aerospace community, and the SIMPLE relaxation method [36], developed for convective–diffusive heat transfer problems by Spalding and Patankar and then refined in a semi-implicit method by Patankar [37]. The MacCormack method is applied to the 2D computation of the edge plasma by Gerhauser and Claassen [9, 10], and the SIMPLE method by Braams [11, 12]. A generalized orthogonal grid adaptation was given for the MacCormack method by Deiwert [38]. Patankar's approach is based on the control volume approach to finite differencing and directly applicable to the required general orthogonal grid.

Based on the computational requirements for the coupled edge plasma–neutral problem, a method based on the SIMPLE relaxation was chosen. The geometry considerations are sketched in III.2 and the basics of the relaxation method are outlined in III.3. The interested reader is referred to Patankars' text [37] for details of the finite differencing scheme and to discussion of its application to a plasma by Braams [12]. The compressible form required for the plasma equations has modest relaxation parameter requirements as discussed in Section III.4 and significant modifications were found necessary to solve for the plasma fluid case. Where our approach differs from the previous efforts, we discuss the method in greater detail, as in solving the density with an "implicit diffusion" method in Section III.5. True steady state solutions require a residual correction (Section III.6). Computational performance is summarized III.7.

III.2. *Geometric Considerations*

Geometries were illustrated for the toroidally symmetric case in Figs. 1–3. New coordinates, x and y, are used in referring to the 2D computational axes in the (θ, r) plane, where x is parallel to the poloidal field, B_θ, and y is in the poloidal flux surface gradient direction. The computational geometry is related to the toroidal metric geometry through the general volume element, dV:

$$dV = dx\, dy\, dz = h_\theta d\theta\, h_r dr\, h_\phi d\phi = h_\theta d\theta\, h_r dr\, 2\pi R \quad (25)$$

which relates each metric element as:

$$\begin{aligned} dx &= h_\theta\, d\theta \\ dy &= h_r\, dr \\ dz &= 2\pi R(\theta, r). \end{aligned} \quad (26)$$

The orthogonal computational grid on the magnetic flux surfaces is generated by one of several preprocessor codes [7]. The preprocessor code reads the poloidal magnetic flux data generated by an MHD equilibria code (the PESTE

[39] and the NEQ [40] MHD codes have been used). An orthogonal computational grid is generated from this data in the (θ, r) plane and at each grid point the magnetic shear is calculated, B_θ/B, to project the parallel momentum into the poloidal plane. The lines of constant poloidal flux are derived directly from fits to the MHD code output data. Several schemes for generating the orthogonal mesh lines along the gradient of the poloidal magnetic flux surfaces have been described [41–43].

In the present study the grid generation method involves an evaluation of linearly piece-wise orthogonal approximations. One moves from a known point (x_0, y_0) on one magnetic flux line segment, S_0, to the point to be determined (x_1, y_1) on the adjacent flux line segment, S_1. These line segments are local linear approximations and must converge or diverge (unless they are parallel then the mutually orthogonal piece is trivially perpendicular to both) and thus they must intersect. A third line which best approximates the orthogonal to the two line segments then forms equal angles with each line segment and the three lines form an isosceles triangle. With this simple trigonometric interpretation of the local orthogonal approximation to the magnetic flux surface gradients, one can construct the entire grid by starting at fixed points along one boundary (e.g., the magnetic separatrix) and marching across the prescribed magnetic flux surfaces covering the plasma edge region of interest. Non-orthogonal target orientation in the (θ, r) plane is modelled by varying the number of grid cells along each magnetic flux surface as seen in Fig. 3.

The finite discretized fluid equations are based on the control volume or integral approach rather than a differential formulation. Through use of the divergence theorem a system of coupled algebraic equations are cast in terms of fluxes normal to each computational cell surface. The divergence theorem equates the volume integral of the divergence of a flux, $\nabla \cdot \Gamma_\xi$, to the closed surface integral of the components of the flux, Γ_ξ, normal to that surface:

$$\int \nabla \cdot \Gamma_\xi \, dV = \int \Gamma_\xi \cdot dA. \tag{27}$$

Integrating the differential equation over the volume of each computational cell, the divergence of flux is expressed conveniently in terms of the flux normal to each of the computational cell's surfaces times the respective surface areas defining the cell boundaries.

This is illustrated with an example, using the continuity equation:

$$\frac{\partial n}{\partial t} + \nabla \cdot (n\mathbf{u}) = S_n(n_0). \tag{28}$$

In toroidal coordinates, $H = h_\theta h_r R$, with toroidal symmetry and including the parallel and drift velocity components, u and w, one finds the continuity equation to be

$$\frac{\partial n}{\partial t} + \frac{1}{H}\left(\frac{\partial}{\partial \theta}\left(n h_r R\left(\frac{B_\theta}{B}u + \frac{B_\phi}{B}w\right)\right) + \frac{\partial}{\partial r}\left(n u_r h_\theta R\right)\right) = S_n(n_0). \tag{29}$$

Integrating this equation over the control volume representing one grid cell, this becomes

$$\frac{\partial n}{\partial t}dV + \frac{dx\,dy\,2\pi R}{h_\theta h_r R}\left(\frac{\partial}{\partial \theta}\left(n h_r R\left(\frac{B_\theta}{B}u + \frac{B_\phi}{B}w\right)\right) + \frac{\partial}{\partial r}\left(n u_r h_\theta R\right)\right) = S_n(n_0)\,dV \tag{30}$$

Substituting in the grid metrics $h_\theta\, d\theta \to dx$ and $h_r\, dr \to dy$ and cancelling coefficients, one obtains

$$\frac{\partial n}{\partial t}dV + 2\pi\, dr\left\{\partial_x\left\{n h_r R\left(\frac{B_\theta}{B}u + \frac{B_\phi}{B}w\right)\right\}\right\} + 2\pi\, d\theta\{\partial_y\{(n u_r h_\theta R)\}\} = S_n(n_0)\,dV, \tag{31}$$

where $\{\partial_x\{\cdot\}\}$ and $\{\partial_y\{\cdot\}\}$ imply finite difference operations on the enclosed terms respectively in the x the y directions. Since $2\pi\, dr$ and $2\pi\, d\theta$ are constant unit lengths (as defined in (25), (26), it is h_r and h_θ which vary with respect to the coordinates), they can be brought back into the finite differenced expressions, where they are combined with the metrics inside the brackets to obtain the metric coefficients in terms of dx, dy, and dz:

$$\frac{\partial n}{\partial t}dV + \left\{\partial_x\left\{n\,dy\,dz\left(\frac{B_\theta}{B}u + \frac{B_\phi}{B}w\right)\right\}\right\} + \{\partial_y\{(n u_r\, dx\, dz)\}\} = S_n(n_0)\,dV. \tag{32}$$

The area elements are given as $dA_{yz} = dy\,dz$ and $dA_{xz} = dx\,dz$. The brackets enclose flux terms which have been integrated over their respective surface areas, so one can write the term, for example, in the x direction as $\{\partial_x\{\Gamma\, dA\}\}$. This last equation simplifies to the more intuitively obvious form we expect for a control volume approach,

$$\frac{\partial n}{\partial t}dV + \{\Gamma\, dA\}_{x+1/2} - \{\Gamma\, dA\}_{x-1/2} + \{\Gamma\, dA\}_{y+1/2} - \{\Gamma\, dA\}_{y-1/2} = S_n(n_0)\,dV, \tag{33}$$

where the plus and minus $\frac{1}{2}$ notation refers to the control volume boundary in the respective directions as shown in Fig. 4.

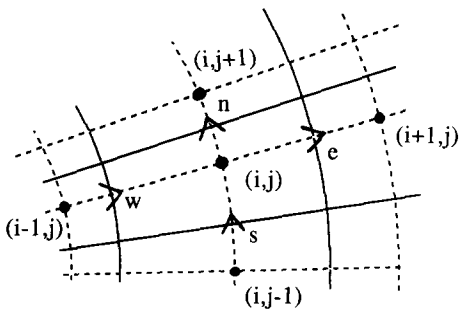

FIG. 4. The computational grid and cell indices.

An orthogonal grid is constructed in the staggered grid form as in Fig. 4 for computation. The transported quantities n, n_0, T are calculated at the main cell center, (i, j), and the fluxes, Γ, and velocities are calculated at the main cell boundaries, denoted: $e =$ east, $(i+\frac{1}{2})$, $w =$ west, $(i-\frac{1}{2})$, $n =$ north, $(j+\frac{1}{2})$, $s =$ south, $(j-\frac{1}{2})$. The control volume for the x component of velocity is staggered one-half of the main grid cell horizontally to the right, and the control volume for the y component of velocity is staggered vertically one-half grid cell to the top in Fig. 4. A piece-wise orthogonal grid is assumed, with straight line approximations between adjacent grid points. Because of the staggered grid, the grid point density is twice the density of the main grid cells in each direction.

Summarizing, the general integral transport equation operator, Z,

$$Z = \int \nabla \cdot (\alpha \mathbf{u}\xi - \beta \nabla \xi)\, dV = \int \nabla \cdot (\Gamma_\xi)\, dV, \tag{34}$$

where ξ is the quantity transported, and Γ_ξ is the flux of ξ from a volume element dV. Cross-field derivatives are ignored, consistent with the assumed simplified momentum viscosity tensor. In the staggered grid, Eq. (34) is written

$$\int \nabla \cdot (\alpha\phi \mathbf{u} - \beta \nabla \phi)\, dV = A_e\Gamma_e - A_w\Gamma_w + A_n\Gamma_n - A_s\Gamma_s, \tag{35}$$

where

$$\Gamma_e = (\alpha u\phi)_e - \beta_e \frac{\partial \phi}{\partial x_e}, \tag{36}$$

$$\Gamma_w = (\alpha u\phi)_w - \beta_w \frac{\partial \phi}{\partial x_w}, \tag{37}$$

and similarly for Γ_n and Γ_s.

III.3. *The Semi-implicit Method*

The relaxation scheme is based on the SIMPLE algorithm [36, 37], an iterative semi-implicit calculation. It is similar to the explicit scheme for pressure relaxation developed by Harlow and Welch in the MAC method [44]. The essence of the pressure relaxation is to combine the continuity and momentum equations as a pressure correction equation, solved on a staggered grid. As iteration for the pressure correction proceeds, the pressure error is reduced to zero and so the residual, equal to the continuity equation, becomes satisfied in the iteration-relaxation process.

To implement the semi-implicit form of the relaxation scheme for the fluid system, first the equations governing the convective–diffusive flux of each of the unknown conserved quantities except density, including velocity, and temperatures, T_i, and T_e, are written in a fully implicit finite differenced form, using Patankar's "power-law" differencing scheme [37]. In this finite differenced form, the sum of the convection term and the time dependent term at the advanced time step is replaced by the product of the conserved quantity times the finite differenced form of the continuity equation. This numerically stabilizes the convective–diffusive flux of each conservation equation as illustrated in the following.

A general form of the convective–diffusive equation can be written:

$$\frac{\partial \gamma\xi}{\partial t} + \nabla \cdot (\alpha\xi \mathbf{u} - \beta \nabla \xi) = S(\xi). \tag{38}$$

This general form equation can be written for plasma temperature, where $\xi = \frac{3}{2}T$, and $\gamma = n$, as

$$\frac{3}{2} n \frac{\partial T}{\partial t} + \frac{3}{2} T \frac{\partial n}{\partial t} + \nabla \cdot \left(n\mathbf{u} \frac{3}{2} T \right) + \nabla \cdot (-\beta \nabla T) = S_T. \tag{39}$$

The continuity equation can then be multiplied by $\xi = \frac{3}{2}T$, to obtain

$$\frac{3}{2} T \frac{\partial n}{\partial t} + \frac{3}{2} T \nabla \cdot (n\mathbf{u}) = \frac{3}{2} TS_n. \tag{40}$$

The advective terms (third term in (39) and second term in (40)) are not analytically identical; however, it has been shown [37] that the finite difference expression for either is equivalent in the power law form of the finite differenced control volume equations. This assumes that the conserved quantity, here T, is constant throughout each computational cell volume. One can then rewrite the plasma temperature equation (39) by combining with Eq. (40) in a finite differenced form which corresponds to a diffusive type equation,

$$\frac{3}{2} n \frac{\partial T}{\partial t} + \nabla \cdot (-\beta \nabla T) = S_T - \frac{3}{2} TS_n, \tag{41}$$

where $\nabla \cdot (-\beta \nabla T)$ represents the finite differenced operator in power law form for the divergence of the diffusive heat flux. This effectively eliminates the numerically unstable convection term while leaving the diffusive term, and gaining a source term, $-\frac{3}{2} TS_n$, from Eq. (40). The source term can be linearized for numerical stability. In applying this method to the plasma equations, the plasma continuity equation contains a significant source term. This is unlike [illegible] source term is zero. The reactive term introduces an extra effective source into the finite differenced form of the equations for each of the conserved quantities, and these must be linearized implicitly.

The flux of the conservative quantities ($u_\parallel$, T_i, T_e) after the "power-law" differencing scheme is solely diffusive and thus is numerically stabilized for an implicit solution with Eq. (41) evaluated at the advanced time step. The usual finite differencing for diffusion (e.g., see Chap. 8 in [45]), using a control volume approach and integrating over the volume, is formulated implicitly for the neutral density assuming plasma source terms which are determined by iteration. One obtains a coupled system of non-linear algebraic equations representing the partial derivatives in two dimensions for each of the unknowns (except density) in the form

$$A_{ij}\xi_{ij} = \Sigma(A_{i\pm1,j\pm1}\xi_{i\pm1,j\pm1}) + B_{ij}, \tag{42}$$

where ξ is the unknown quantity at the advanced time step, the summation is over adjacent grid cells and represents the divergence of the flux of the unknown quantity in the usual five-point form for a 2D problem. Sources are evaluated at the advanced or implicit time step. Inhomogeneous sources and the conserved quantity at the present time step are included in B_{ij}. The flux divergence terms are separated into the orthogonal components, indexed here with i and j, and then Eq. (42) is solved with simple tridiagonal sweeps, successively in each direction, as in a "line-SOR" method [46]. The time step plays the role of a relaxation parameter.

In the SIMPLE relaxation of the momentum equation, the source term, B_{ij}, is separated into the pressure gradient, ∇P_{ij}, and all other source terms, S_{ij},

$$A_{ij}\xi_{ij} = \Sigma(A_{i\pm1,j\pm1}\xi_{i\pm1,j\pm1}) + \nabla P_{ij} + S_{ij}, \tag{43}$$

where ξ now represents a component of momentum (or fluid velocity). The flow velocities and the pressure are successively relaxed until a residual equal to the pressure error approaches zero. The zero residual corresponds to the condition that the present iterate value for density approaches the correct density and so the continuity equation is satisfied to within a specified tolerance.

III.4. *The Semi-implicit Method for a Compressible Fluid*

The relaxation method of Patankar is derived for the incompressible fluid or constant density case but can be extended to a compressible fluid with some added terms complicating the pressure error equation. The pressure is related to the density and temperature in a plasma as, $p = nkT$, where the density and pressure vary as a function of space. The pressure relaxation of the plasma must take [illegible] pressible form of the relaxation scheme must be used in solving for plasma flows.

The relaxation scheme is based on an iteration to the implicit solution in which each unknown (n, $\mathbf{v}$) is corrected while assuming the others are constant, equal to their previous iterate values. One can write the actual solution as the sum of the iteration solution and the error of the iteration solution. To relax the continuity equation in 2D one defines

$$\begin{aligned} n &= n^g + n' \\ u &= u^g + u' \\ v &= v^g + v', \end{aligned} \tag{44}$$

where the superscript g refers to the iteration (guessed) solutions, the prime indicates the error terms, and the left sides of the equations are the correct solutions. The inhomogeneous plasma continuity equation is simplified for discussion purposes in the form:

$$\frac{\partial n}{\partial t} + \frac{\partial (nu)}{\partial x} + \frac{\partial (nv)}{\partial y} = nn_0 \langle \sigma v \rangle_{ei}. \tag{45}$$

Substituting the above iteration solutions and errors into this equation for continuity, we obtain an "iteration" continuity equation:

$$\begin{aligned} &\frac{\partial (n^g + n')}{\partial t} + \frac{\partial}{\partial x}((n^g + n')(u^g + u')) \\ &\quad + \frac{\partial}{\partial y}((n^g + n')(v^g + v')) \\ &\quad = (n^g + n')\, n_0 \langle \sigma v \rangle_{ei}. \end{aligned} \tag{46}$$

Errors are assumed to be small, so the products of error terms are dropped. Rearranging, we have

$$\begin{aligned} &\frac{\partial (n')}{\partial t} + \frac{\partial}{\partial x}((n^g u' + u^g n')) \\ &\quad + \frac{\partial}{\partial y}((n^g v' + v^g n')) - (n')\, n_0 \langle \sigma v \rangle_{ei} \\ &\quad = -\frac{\partial n^g}{\partial t} - \frac{\partial (n^g u^g)}{\partial x} - \frac{\partial (n^g v^g)}{\partial y} \\ &\quad + n^g n_0 \langle \sigma v \rangle_{ei}, \end{aligned} \tag{47}$$

where we have also simplified, by neglecting the error in the neutral density, $n_0 = n_0^g + n'$, and the error in the temperature dependent reactivity of the electron impact ionization.

It is at this point in Eq. (47) that one can neglect all terms involving n' for the incompressible fluid case, since then density is a known value and $n \to n^g$. In that case the SIMPLE method prescribes the velocity errors in (47) in terms of gradients in the density (or pressure) errors, $u'(n' = p'/kT)$ and $v'(n' = p'/kT)$, as we show in the following equations. The resulting equation for n' (or for p' as in [37]) is a Poisson-like equation for the incompressible fluid case, it is purely diffusive and therefore numerically stable for implicit solution. Unfortunately in the plasma case, the extra terms related to compressibility must be retained.

The error terms must be expressed in a form such that iterations converge and as the errors approach zero, the LHS of Eq. (47) goes to zero and the RHS, or residual, equals the correct continuity equation. The desired form of the error terms is to make the convective error terms look like diffusive terms to stabilize the numerical computation. To do this, each error term is written in terms of a gradient with the velocity errors in terms of the pressure gradient errors. The momentum equation for parallel velocity, u, at point (i, j) in the finite difference form (43), is written

$$A_{ij}u_{ij} = \Sigma(A_{i\pm1,j\pm1}u_{i\pm1,j\pm1}) - \frac{\partial(nT)}{\partial x} + B_{ij}, \qquad (48)$$

where the second term on the right is the pressure gradient and B_{ij} is any remaining source term. The pressure gradient is assumed to dominate the errors so that the divergence term and the source term, B_{ij}, are neglected in the pressure correction (but not in the momentum equation solution). Temperature is also held constant during the pressure relaxation, which allows us to rewrite Eq. (48), solving for the velocity error term, u', in terms of the density error, n',

$$u'_{ij} \approx -\frac{1}{A_{ij}}\frac{\partial(n'T)}{\partial x}. \qquad (49)$$

An estimate of the radial velocity error, v' in terms of n', comes from the radial flux equation (3):

$$v' \approx -\frac{D_{an}}{n}\frac{\partial n'}{\partial y}. \qquad (50)$$

Substituting these error terms back into Eq. (47), we obtain the density error (pressure relaxation) equation similar to that given previously [12]:

$$\frac{\partial(n')}{\partial t} + \frac{\partial}{\partial x}\left(-n^g\frac{1}{A_{ij}}\frac{\partial(n'T)}{\partial x} + u^g n'\right) + \frac{\partial}{\partial y}\left(-n^g\frac{D_{an}}{n}\frac{\partial n'}{\partial y} + v^g n'\right) - (n')\,n_0\langle\sigma v\rangle_{ei} = -\frac{\partial n^g}{\partial t} - \frac{\partial(n^g u^g)}{\partial x} - \frac{\partial(n^g v^g)}{\partial y} + n^g n_0\langle\sigma v\rangle_{ei}. \qquad (51)$$

This is in the desired diffusion form, but unlike the incompressible case which is purely diffusive, there are now also advective terms present due to the compressibility of the plasma. These may be implicitly unstable if the advection dominates, leading to a matrix of the discretized equations which is not diagonally dominant. The neutral source term is also destabilizing, since it is positive and can increase the density. In the high recycling regimes this source term dominates the continuity balance.

Results obtained by relaxing Eq. (51), with the coupled equations, (42) for each of the conserved quantities and with the neutral equations, are satisfactory. The relaxation must be done slowly (small relaxation parameter or time step) due to the nonlinearities. Therefore a method, involving "semi-implicit diffusion" for solving the continuity equation was examined for improvement in relaxation performance.

III.5. *Semi-implicit Diffusion Closure*

Computational time requirements and numerical instabilities in the previous relaxation scheme provided motivation to solve the continuity equation and close the equation system by an alternative scheme, referred to as the semi-implicit diffusion method. The conserved quantities, u, T_i, and T_e, are still solved using the power law differencing scheme.

The essence of the semi-implicit diffusion closure method is to add a "diffusion" term to both the right-hand side and the left-hand side of the continuity equation and to iterate on the solution, so that in iterating, the density guess, n^g, approaches the correct density, n. In this iteration process, the diffusion terms on each side of the density equation cancel each other and only the advective terms of the continuity equation remain. The method is similar to "artificial viscosity" used for stabilizing advective momentum equations [47] and similar to a semi-implicit method developed for solving the fluid MHD equations [48].

The radial velocity for the plasma has already been assumed to be diffusive by the assumptions of an anomalous transport, so the radial transport is implicitly stable and does not require numerical stabilization. The advection component requiring numerical stability in the plasma continuity equation is along the B field (along x in this case).

Using the "implicit diffusion" coefficient, D_{id}, the form of the continuity equation in 1D is

$$\left(\frac{\partial n}{\partial t}+\frac{\partial (nu)}{\partial x}+\frac{\partial}{\partial x}\left(-D_{id}\frac{\partial n}{\partial x}\right)\right)^{m+1} = \left(nn_0\langle\sigma v\rangle_{ei}+\frac{\partial}{\partial x}\left(-D_{id}\frac{\partial n}{\partial x}\right)\right)^{m}, \quad (52)$$

where m is the current iteration index (*not* the time step index; all quantities are evaluated implicitly at the next time step) and $m+1$ is the next or implicit iteration step. The source term, $nn_0\langle\sigma v\rangle_{ei}$, must be retained on the RHS because it is positive and could be destabilizing during iterations if solved implicitly on the LHS. In iterating, the value of density at m approaches that at $m+1$, and the implicit diffusion on the LHS approaches the explicit diffusion on the RHS. In the limit of $n^m \to n^{m+1}$, the diffusion terms on each side cancel and the equation approaches the correct continuity equation.

The advantage in adding this diffusion is that the magnitude of this additional term can be selected to equal or exceed the convective term in the continuity equation. This effectively stabilizes the continuity equation with a diffusive term and allows for implicit numerical solution. Numerical stability is guaranteed for

$$D_{id} \geqslant u\,dx. \quad (53)$$

Taking the equality case of (53) and using the power-law differencing scheme on the above form of the continuity equation (52), this method is similar to an implicit "upwinding scheme," since the downwind contribution will be exactly cancelled by the implicit diffusion from the "downwind" grid cell.

In testing the implicit diffusion scheme, it is confirmed that the density equation alone is numerically stable and can be advanced as expected in a fixed flow field (i.e., not iterating on velocity or temperatures) with relatively few iterations and arbitrarily large time steps. The numerical dispersion was examined qualitatively by applying Eq. (52) to a test problem, the 1D advective propagation of a square wave at a constant velocity. Dispersion, related to the spreading of the pulse shape in time, was found to be comparable to that of an "upwinding" difference scheme.

III.6. *Residual Corrections*

In either density-closure method, it was found necessary to take large numbers (a few hundred to a few thousand) of time steps to achieve convergence in a full simulation, starting from a low density and low temperature plasma and continuing to steady state in a full recycling solution. This results from the combination of a small time step ($\approx 10^{-5}$ s) limited by plasma parallel flow into the target, and the large total time (several milliseconds for the fixed boundary condition (BC) cases, and tens of milliseconds for flux BC) needed to achieve a steady solution. The total time is fixed by the buildup of the recycling regime which is limited in turn by the growth of neutral density recycled from the core and from the vacuum duct regions. Neutrals, re-ionized in the core, return to the edge through the relatively slow radial transport. The neutrals returning from the duct also have a long effective buildup time and contribute to the relatively slow equilibraton of the recycling regime in the edge plasma. Thus the coupled problem must proceed at the plasma-limited time step size, but over the neutral-limited total time to achieve steady state.

The large number of required time steps with an iteration error at each time step can lead to large accumulated errors if not properly treated. Consider a relative error of 10^{-3} allowed at each of 2000 time steps. If the error is consistently biased in one direction, as it usually is in the plasma for physical reasons, then the accumulated error after the 2000 time steps will be of the order:

$$\text{err} \approx O(1.001)^{2000} = 7.4, \quad (54)$$

or the solution will change by several times its own magnitude! Under these conditions the solution will not appear to converge to a constant or steady state value, but will converge to the "error rate" of change implied by the accumulating error. Thus the solution will appear to "drift" continuously in time without clearly achieving steady state.

This problem was dealt with by Hirt and Harlow [49] in a corrective procedure for the numerical solution of non-linear initial value problems (IVP). Generally, one has a matrix of IVP equations:

$$\frac{\partial \Omega(\xi)}{\partial t}+\Gamma(\xi)=0, \quad (55)$$

where ξ is the unknown vector, and $\Omega(\xi)$ and $\Gamma(\xi)$ are functions of the unknown vector. This is written, instead, as two coupled equations,

$$\frac{\partial D}{\partial t}=\frac{\partial \Omega(\xi)}{\partial t}+\Gamma(\xi) \quad (56)$$

and

$$D=0, \quad (57)$$

where D is the residual error term. This should be identically zero, but is not zero in an iterative calculation for a non-linear problem. The residual magnitude is comparable to the error tolerance specification. In the above form, this

admits a nonzero rate of error in $\partial D/\partial t$ and imposes the additional constraint that the error at the new time, D, should be equal to zero, which provides us with a basis to correct successive iterations using the previous iterate error.

The original correction was formulated for an explicit time step, but is modified here for an implicit calculation. In an implicit finite difference form, stepping in a time interval, δt, from time, n, to time, $n+1$, one obtains

$$D^{n+1} = D^n + \Omega(\xi^{n+1}) - \Omega(\xi^n) + \delta t \cdot \Gamma(\xi^{n+1}) \quad (58)$$

and

$$D^{n+1} = 0. \quad (59)$$

Combining these gives the implicit time step solution for ξ^{n+1}, in the form,

$$\Omega(\xi^{n+1}) + \delta t \cdot \Gamma(\xi^{n+1}) = +\Omega(\xi^n) - D^n, \quad (60)$$

where D^n is evaluated by decrementing the time step index in Eq. (58), giving

$$D^n = D^{n-1} + \Omega(\xi^n) - \Omega(\xi^{n-1}) + \delta t \cdot \Gamma(\xi^n). \quad (61)$$

These last two equations are rewritten to be consistent with the notational form given previously,

$$(A_{ij}\xi_{ij} - \Sigma(A_{i\pm1,j\pm1}\xi_{i\pm1,j\pm1}))^{n+1} = B_{ij}^{n+1} - \frac{D^n}{\delta t}, \quad (62)$$

where the previous error term is evaluated as:

$$\frac{D^n}{\delta t} = \frac{D^{n-1}}{\delta t} + (A_{ij}\xi_{ij} - \Sigma(A_{i\pm1,j\pm1}\xi_{i\pm1,j\pm1}) - B_{ij})^n. \quad (63)$$

The previous time step values as $(n-1)$, denoted in (61) as $\Omega(\xi^{n-1})$, have been incorporated into the term $(B_{ij})^n$ in (63), consistent with the decremented time index.

This correction is implemented in the plasma edge code for the density only. It was found that applying this residual correction to the other variables, T_i, T_e, or n_0, was unnecessary and led to a more numerically unstable situation in some cases.

IV. COMPUTATIONAL PERFORMANCE, INITIAL CONDITIONS, AND CONVERGENCE

The coupled plasma–neutral equations are solved in the code, EPIC (edge plasma implicit computation) [10]. There are three types of geometry inputs possible. Rectangular geometry (a first approximation to the SOL geometry) with variable grid spacing is directly read by the EPIC code. Orthogonal grid surfaces for limiters (θ, r) and for approximate divertor geometries are generated analytically in a preprocessor code. A grid in magnetic flux geometry for accurate divertor representation is generated from PESTE [39] or NEQ [40] MHD equilibria data using a second preprocessor code [7] as in Fig. 3.

The output data from the EPIC code is plotted as a function of time at two representative points (one upstream along the separatrix and one at the separatrix–target intercept) as a useful and rapid check on convergence and the time dependent evolution. Additional graphics postprocessors can generate various types of plots displaying spatial distributions of the solution at selected times.

Each unknown is solved on the 2D computational grid by first sweeping horizontally in an implicit "line-SOR" procedure to pick up the sheath boundary condition and then sweeping vertically to pick up the core–SOL boundary condition. Each sweep involves the fully implicit solution, successively, along each line, using updated values as soon as available. The equations are solved for each unknown, successively updating the solutions at the new time step as available.

The order of solution in the implicit diffusion scheme for the coupled variables is n_0, n, $v(n)$, T_i, T_e, u. After solving the coupled variables, the dependent quantities: plasma potential, drift velocity, and total poloidal velocity are computed. The neutral density is solved first because it is diffusive and numerically stable, and it is needed in the source term for the continuity equation. The temperatures are solved before the parallel velocity because the sonic boundary condition on u depends on T (target). The successive solution of each unknown quantity limits the technique to a semi-implicit status. Iterating to convergence at each time step recovers an implicit method.

Iterating the coupled system of plasma and neutral equations with excessively large relaxation, corresponding to time steps exceeding a value of the order (10^{-5} s) leads to numerical instabilities. This time step is about one order of magnitude larger than would be allowed by the CFL criterion for the explicit treatment of advection and is much larger than the time step allowed by explicit treatment of the diffusive terms. The observed time step limit is related to the non-linear interactions and the sequential solution of each unknown within one iteration. The parallel sound speed boundary condition (BC) at the target grid cells couples the densities and flow field explicitly to the plasma temperatures. This coupling in the sheath BC of velocity and the temperature appears to be the limiting factor for time step size stability. Because of this coupling, numerical instabilities have been observed to oscillate in some cases with frequencies that are characteristic of sound or pressure waves, but that are numerical and not physical in origin.

Early trials with the code were iterated to convergence at each time step (i.e., fully implicit). Using convergence criteria typically $\Delta u/u$ per step $\approx 10^{-3}$, where the maximum

$\Delta u/u$ is evaluated for each unknown, convergence required on the order of 5–20 iterations per time step, usually settling down to ≈ 5–7 after several steps. It was found by reducing the maximum number of iterations allowed at each time step, that the same solution in time would result with as few as two iterations per time step. This became the "standard run procedure," two iterations per time step, and in this regard the method is like a predictor–corrector scheme with both steps computationally similar, except that in the second step the coefficients have been updated once to values at the new time step.

The first computational time step in a new problem is unique, a "catch-22 situation," wherein one needs to start from a solution which is a self-consistent initial condition, but a self-consistent solution is what one is trying to calculate. At the first time step a guess is provided, either constant profiles at low density and low temperature conditions, or with axial (poloidal) profiles if an axial scale length of plasma density is specified. Consistency with the sheath boundary condition forces plasma pressure at the target to be half the upstream pressure for the initial guess. Several iterations (typically 5–20) at this first time step proceed to be assured that the first step iterates to a self-consistent initial condition. This initialization allows the plasma to equilibriate along the field lines, while the cross-field solution remains relatively flat, reflecting the slower cross-field transport.

Convergence testing for the steady state solution uses a tolerance, *tol*, criteria typically $\Delta u/u \leqslant tol \approx 2. \times 10^{-4}$. Convergence is also monitored with time dependent plots which are useful to determine if an unconverged solution is near

reveal a solution which is slowly drifting away from a true steady state solution. This may be the case even when the residuals at each step appear to be small, satisfying $\Delta u/u \leqslant tol$. In either case the time dependent plots are useful diagnostic tools.

The time to converge is problem dependent, varying with the total time required for the physics to reach steady state divided by the timestep. The timestep magnitude is limited to about 10^{-5} s for the typical problem on a 20×10 grid, which employs a minimum poloidal grid spacing of about 2–5 cm. Adding more grid cells without reducing the size of the smallest (time step limiting) cells will linearly increase the solution time. Making a smaller poloidal grid size near the target proportionately reduces the maximum stable time step. High recycling regimes where plasma and neutral densities are large at the target can be non-linearly destabilizing and in some cases requires halving the time step to maintain stability after the densities are above a critical level (plasma density on the order of 10^{20} m^{-3}). Computational time for the typical problem is about one Cray cpu minute per millisecond of plasma simulation time. This is for unvectorized code, where it is expected that vectorizing the main computational loops may reduce the computational time by up to an order of magnitude.

Flux boundaries are prescribed as a function of time with characteristic time constants of the order of the response time of the SOL recycling so that a quasi-equilibrium can be maintained to simulate a "start-up" condition. It is not computationally practical to simulate real start-up time scales on the order of several seconds, but the simulations are "time-dependent realistic" over the tens of milliseconds required in the SOL plasma to reach steady state.

The required computational time is dictated by the time to establish recycling and particle equilibrium so that the total time is proportional to the device size. This can range from a few milliseconds for fixed value boundary conditions on a small limiter device to several tens of milliseconds for flux boundary conditions at the core–SOL of a large divertor machine and for a simulation from "start-up" conditions (low plasma densities and temperatures far from the steady state solution). It was found that the time to reach steady state solution for fixed value BC (at the core–SOL) on limiter cases range from 2–4 ms. on the CCT (UCLA's tokamak) to 7–12 ms on TEXTOR : ALT-II (a tokamak at Jülich, Germany) [7]. The larger time in the Textor case is due to the wider SOL than usual, 12 cm. On divertors with fixed BC, the total simulation times were 5–8 ms. The flux BC on divertors typically run 20–30 ms for a complete simulation from initial conditions and about 5–7 ms to reach a new equilibrium solution from a similar previous equilibrium solution. The cpu time in minutes is comparable to the simulation time in milliseconds.

Numerical instabilities in the target area result if [illegible]

velocity fields while assuming the temperature is constant during one iteration. This assumption is poor at the target boundary condition, where the velocity approaches the sound speed, a function of the local temperature. It may be possible to improve convergence time by increasing the time step with additional quasi-linearization incorporating the sound speed at the target into the boundary condition on the parallel flow velocity. This possibility was examined briefly in this study, but the attempted quasi-linearizations were not adequate to improve the time step limitation.

V. COMPUTATIONAL RESULTS

V.1. *Calibrations*

Calibration studies have been described elsewhere in several cases [7, 23]. One case involves the validation of the neutral diffusion model, with the one group-ion temperature equilibrium (OGITE) approximtion, incorporated into the EPIC code. It was shown [23] that in a wide range of plasma regimes in density and temperature profiles typical of the tokamak plasma region, the neutral diffusion

model compared well with Monte Carlo transport calculations by the DEGAS [50] code. These tests were in edge plasma regimes, where the plasma which recycled from the target plate was the dominant source of neutrals. In this case the OGITE assumption is reasonably accurate and produces good neutral density results in the diffusion model. In a regime dominated by cold molecular neutrals such as in a strong gas puffing source in the edge, it is likely that a more elaborate neutral diffusion model is required for realistic results, possibily a two goup neutral diffusion model including neutral energy equations to evaluate the average fluid energy of each neutral group.

Calibration studies have also compared the EPIC code results to the computational results of a widely used plasma edge fluid transport code, B2, developed by Braams [12]. Comparisons made in the experimental tokamak plasma regime (ASDEX tokamak) were found to be quite good, with predicted recycling densities and temperatures at the divertor target plate agreeing within 20% between the two codes [7, 23]. These comparisons were fixed value boundary conditions at the separatrix. Related studies using the EPIC code suggested that flux boundary conditions gave more realistic solution profiles.

Comparisons between these codes were made in the tokamak plasma edge regime expected in fusion reactor relevant plasmas [51]. Results from the EPIC code for this case are discussed in the next section. In this regime there is considerably more difficulty in obtaining a stable converged solution with the EPIC code or with the Braams' (B2) code, and so the code comparisons are ambiguous in the power reactor plasma. In these high heat flux regimes, it is difficult to prove that a low temperature divertor plasma solution is stable, so the computational difficulties may represent a physically unstable plasma. Before meaningful code com-

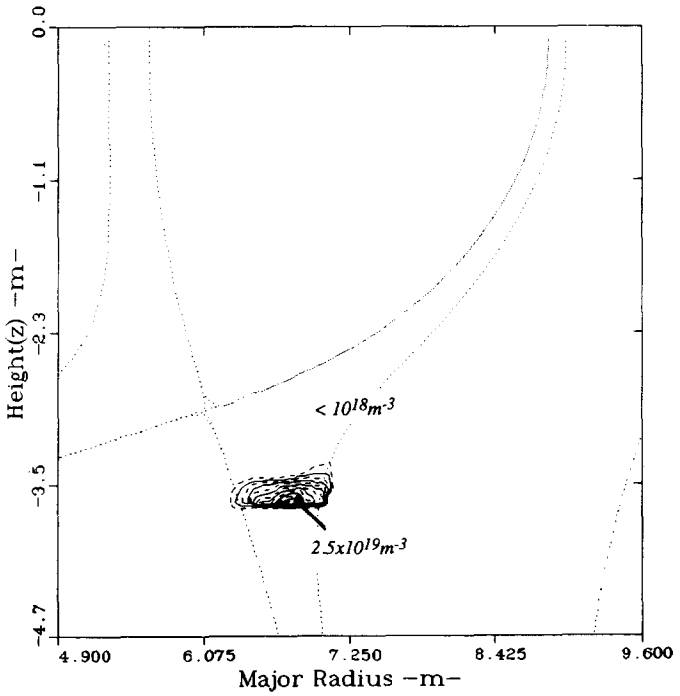

FIG. 5. The neutral density, n_0, recycling solution maximum of $2.5 \times 10^{19}\ m^{-3}$ occurs at the orthogonal target plate about two-thirds of the way radially from the separatrix to the outermost flux surface in the outboard lower scrape off layer. Beyond the contour region, $n_0 < 10^{18}\ m^{-3}$.

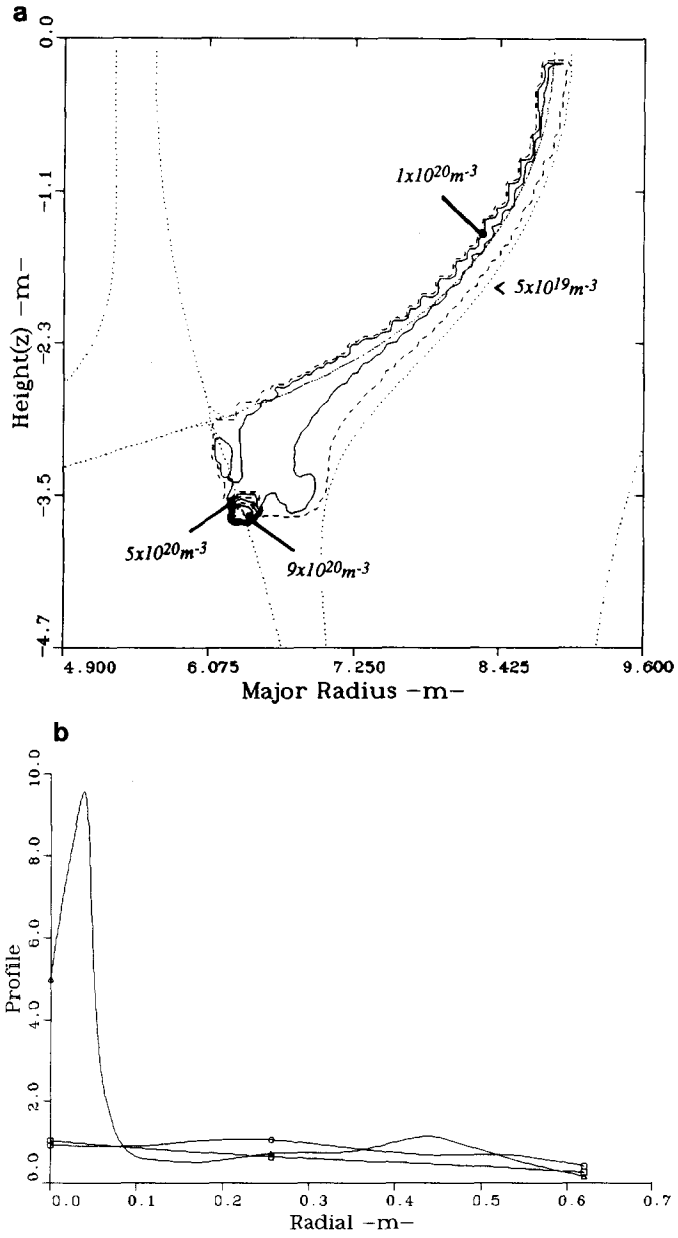

FIG. 6. (a) The plasma density recycling solution peaks sharply with a maximum of $9 \times 10^{20}\ m^{-3}$ near the separatrix and in front of the target. The density is about $1 \times 10^{20}\ m^{-3}$ along the separatrix from the midplane to the x-point, $5 \times 10^{20}\ m^{-3}$ at the separatrix–target intercept, and less than $5 \times 10^{19}\ m^{-3}$ along the first wall (or outermost flux surface), as seen in Fig. 6b. (b) The plasma density solution ($10^{20}\ m^{-3}$) shown radially across the magnetic flux surfaces at three poloidal locations: (□: upstream (midplane), ○: midstream (slightly upstream of the x-point), and △: downstream (across the divertor target).

parisons can be done in this regime, more research is required to distinguish the numerical from the physical instabilities and to resolve the uncertainty in attaining (time dependent) and maintaining (steady state) a low temperature divertor plasma under high power flux conditions.

Calibration by comparison of computational results to observed experimental profiles is limited, due in part to a sparsity of data in the plasma edge. The present code has been compared to data sets taken from two limiter tokamaks, TEXTOR with the toroidally symmetric belt limiter, ALT-II, and the CCT (UCLA). In both of these cases, the comparison was complicated by the flow dynamics in which the poloidal drift appears to play a dominant role [7].

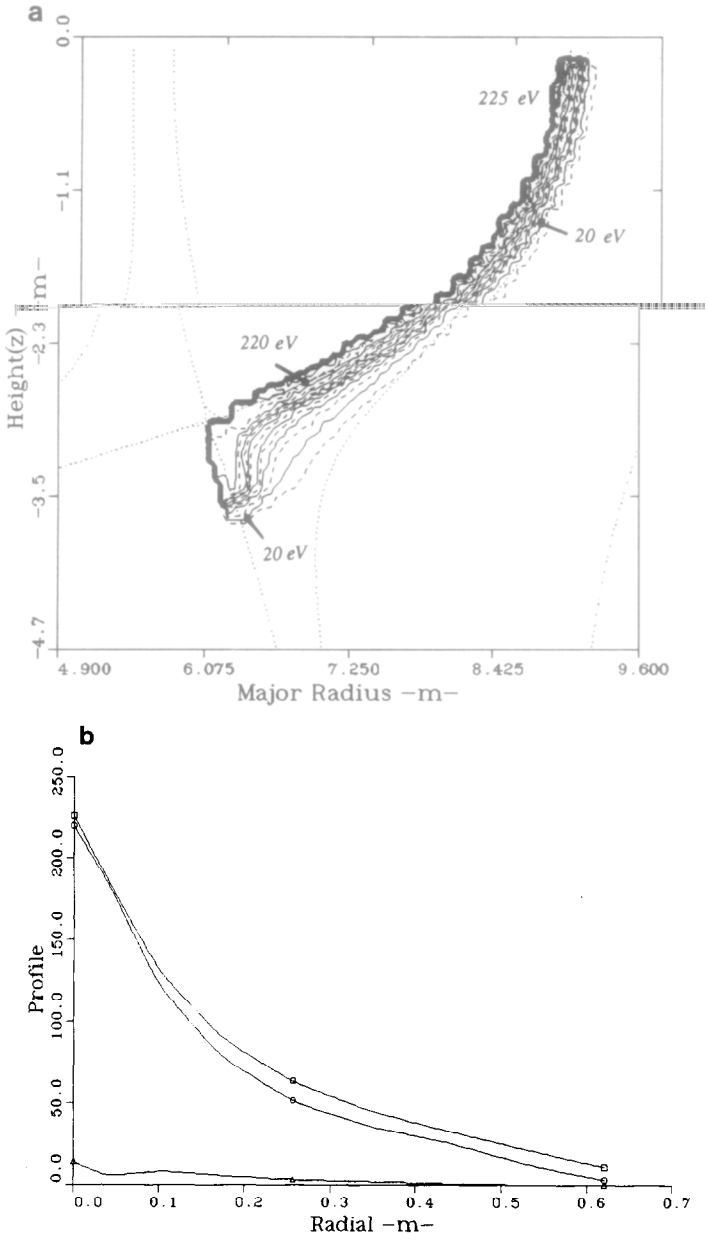

FIG. 7. (a) Electron temperature contours have a maximum along the separatrix of 220 eV (midstream) to 225 eV (upstream). The maximum at the target is 20 eV on the separatrix-target intercept. Values at the first wall are less than 20 eV. (b) Electron temperature solution (eV) shown radially across the magnetic flux surfaces at three poloidal locations: (□: upstream (midplane), ○: midstream (slightly upstream of the x-point), and △: downstream (across the divertor target).

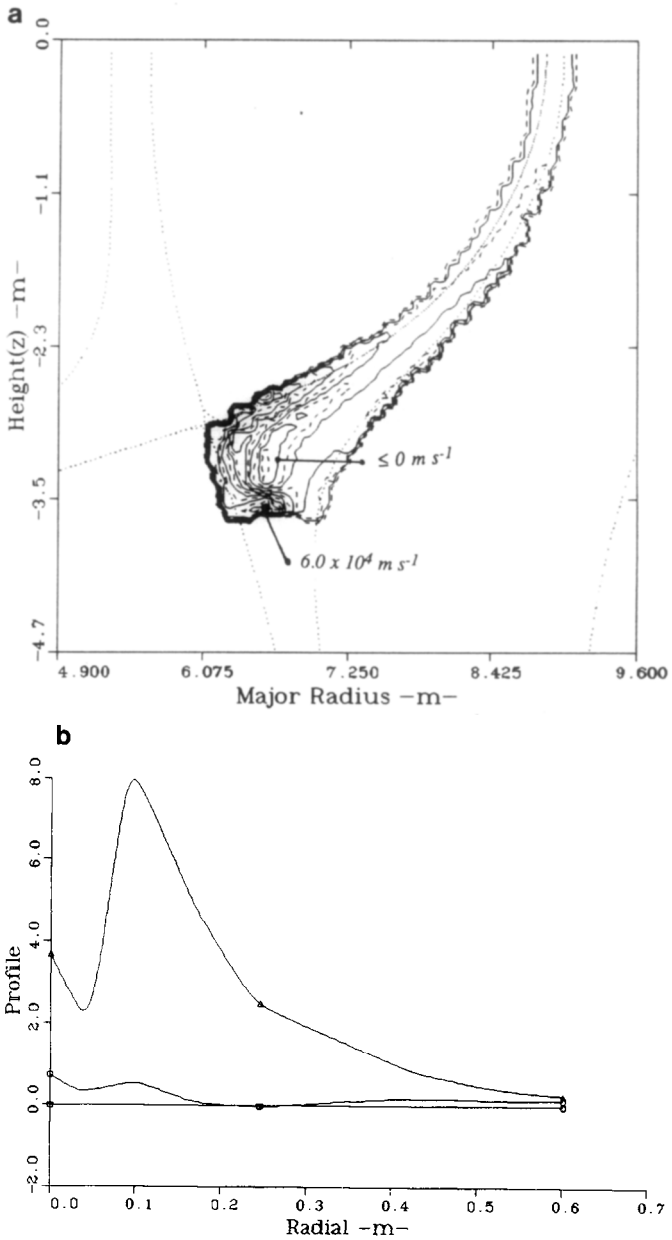

FIG. 8. (a) The plasma parallel velocity solution is near zero throughout much of the scrape off layer except in the divertor region, where it climbs steeply in front of the target to reach a maximum of about 8×10^4 ms^{-1} at the divertor target. A small "stagnant region" ($u \leqslant 0$ ms^{-1}) is indicated in the figure and can be compared to the result in Fig. 8b. (b) The plasma parallel velocity solution (10^4 ms^{-1}) shown radially across the magnetic flux surfaces at three poloidal locations: (□: upstream (midplane), ○: midstream (slightly upstream of the x-point), and △: downstream (across the divertor target).

The calibration of the anomalous radial diffusion coefficient depends on the proper poloidal flow which has a parallel and drift component. Since the present computational model only includes the parallel component of the poloidal flow self-consistently, it is not possible to fully reconcile the computational predictions with the experimental data until the drift flow is self-consistently computed in the model. However, the limiter studies clearly show that the computations and experiments are in reasonable agreement. Further, it is seen that including the drift in the computations is expected to improve computational–experimental comparisons to a level of very good agreement. Similar findings comparing computations to experimental data from the TEXTOR edge plasma have been reported in a self-consistently computed non-ambipolar flow that includes drift flux [9].

V.2. *Model Results for a Divertor Tokamak*

Qualitative results from the EPIC code are shown in Figs. 5–11 for a divertor tokamak proposed to operate in the [illegible] the ARIES (advanced reactor innovations and evaluation study) I reactor [51], which operates in a plasma regime and is sized similarly to the ITER (international tokamak experimental reactor) device [52]. Zero radial advective flux is assumed for this example.

The contour results are computed and plotted in the magnetic geometry for the device, which is determined from the MHD equilibria code, NEQ [40]. The figures show the lower outboard quadrant of the edge plasma or SOL for the device. The outboard midplane is the symmetry line with respect to the parallel flow for this double null configuration. The divertor target (not shown) is orthogonal in this case and located horizontally and below the null (or x-point) at $z = -3.7$ m, where the densities are seen to peak in the neutral and plasma contour plots, Figs. 5 and 6, respectively. The contour plots in each of the resultant figures are seen to extend slightly beyond the actual SOL domain, and to exhibit "wiggles" along the edges, notably along the separatrix. These are minor artifacts of the contouring routine and do not have a physical significance.

The plots of neutral density and plasma density show the recycling near the divertor target, leading to a plasma density maximum near $9. \times 10^{20}\ \mathrm{m}^{-3}$ (in Fig. 6b). There is a concomitant decrease in the plasma temperatures near the divertor target plate, as seen in Figs. 7a and b for the electron temperature. The reduced plasma temperature at the [illegible] sensitive plasma sputtering and erosion of the target material, as discussed for the ARIES reactor [51].

The stability of this desired solution was found to be uncertain in time dependent studies of the plasma edge, suggesting this solution may not be a true steady state

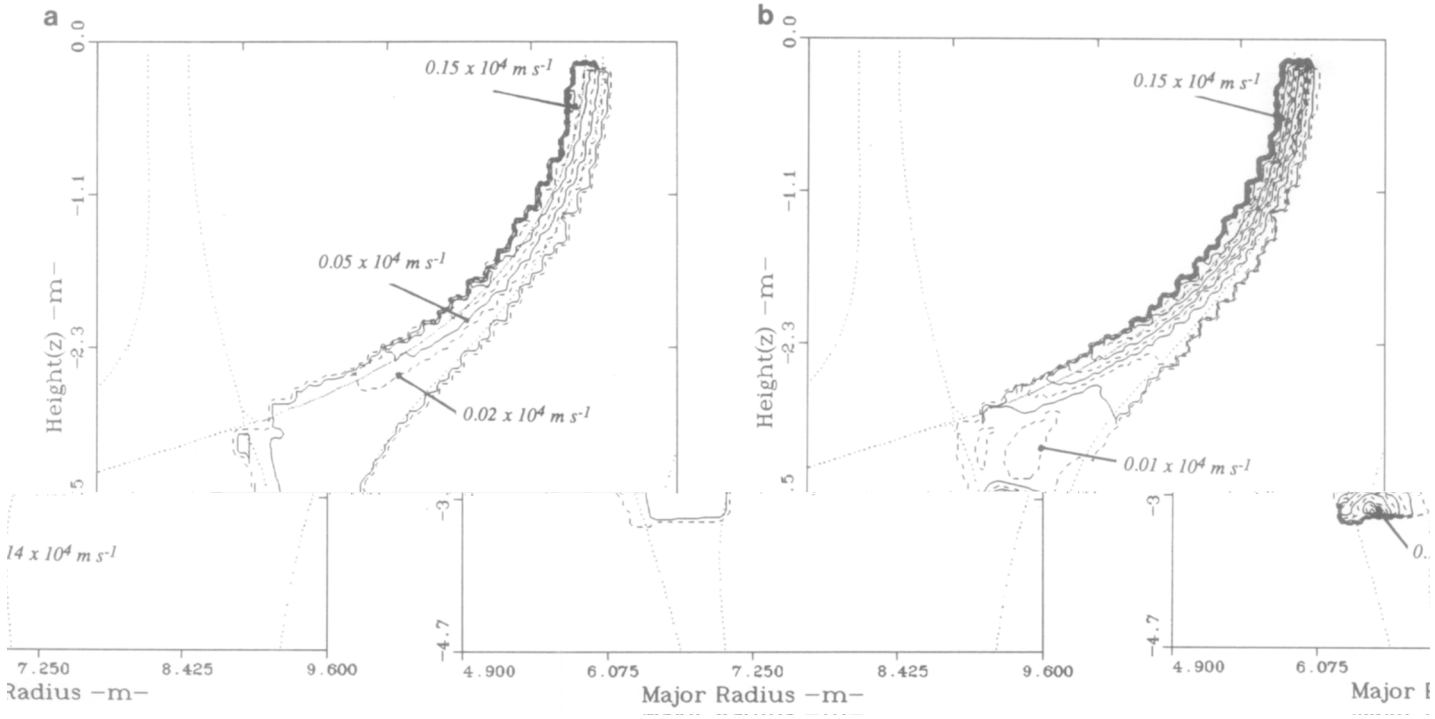

FIG. 9. (a) The plasma drift velocity solution in the outboard lower scrape off layer is characterized by steep radial gradients and mild poloidal gradients, with the solution at the separatrix ranging from $0.05 \times 10^4\ \mathrm{ms}^{-1}$ (midstream) to $0.15 \times 10^4\ \mathrm{ms}^{-1}$ (upstream) and less than $0.02 \times 10^4\ \mathrm{ms}^{-1}$ near the outermost flux surface and throughout the divertor region. (b) The plasma poloidal velocity solution is similar to the drift solution outside of the divertor region and picks up a significant contribution from the parallel flow in the divertor as seen by comparing this figure to Figs. 8a and 9a.

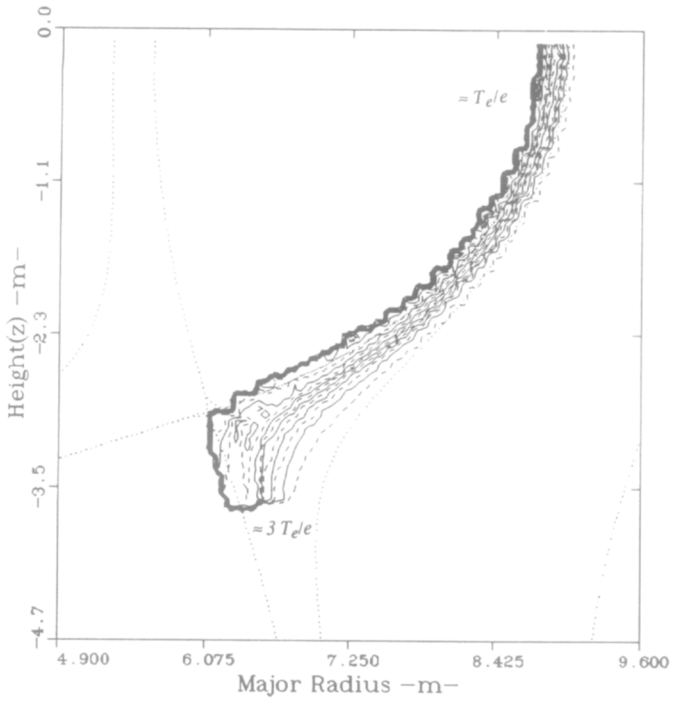

FIG. 10. The ambipolar plasma potential solution approximately follows the electron temperature contours in the outboard lower scrape off layer, ranging from $\approx T_e/e$ (midstream and upstream) to $\approx 3T_e/e$ at the target.

suitable for reactor operation. Additional study in this area is required to gain confidence in obtaining and maintaining the high recycling solution at power reactor flux levels.

The parallel flow has reversed in an area upstream of the maximum recycling zone near the target as seen in the Figs. 8a and b. The double peak in parallel velocity at the target (Δ in Fig. 8b) arises from separate temperature peaks in the ion and electron channels, further evidence of an unstable solution. The drift flow is shown in Fig. 9a and is seen qualitatively to dominate near the separatrix region, where the radial profiles are large. The poloidal flow components of the parallel and drift velocities are combined in Fig. 9b. Recall that the drift flux is calculated from the $E \times B$ and $\nabla p \times B$ drift terms, where E is determined in an ambipolar approximation, and that the drift flux is neglected in the transport of the plasma density and temperatures as a numerical simplification. The figure shows that this simplification is not well justified near the separatrix and efforts to incorporate the drift transport self-consistently have been initiated.

The ambipolar plasma potential and resultant plasma electric fields are shown in Figs. 10, 11a, and 11b. Qualitatively, the radial electric field (with a maximum of order 2×10^4 V/m) is seen to dominate upstream where the drift current is important while the poloidal electric field (of order 100 V/m) is more obvious near the target where the parallel flow gradients are strongest. The electric field in the

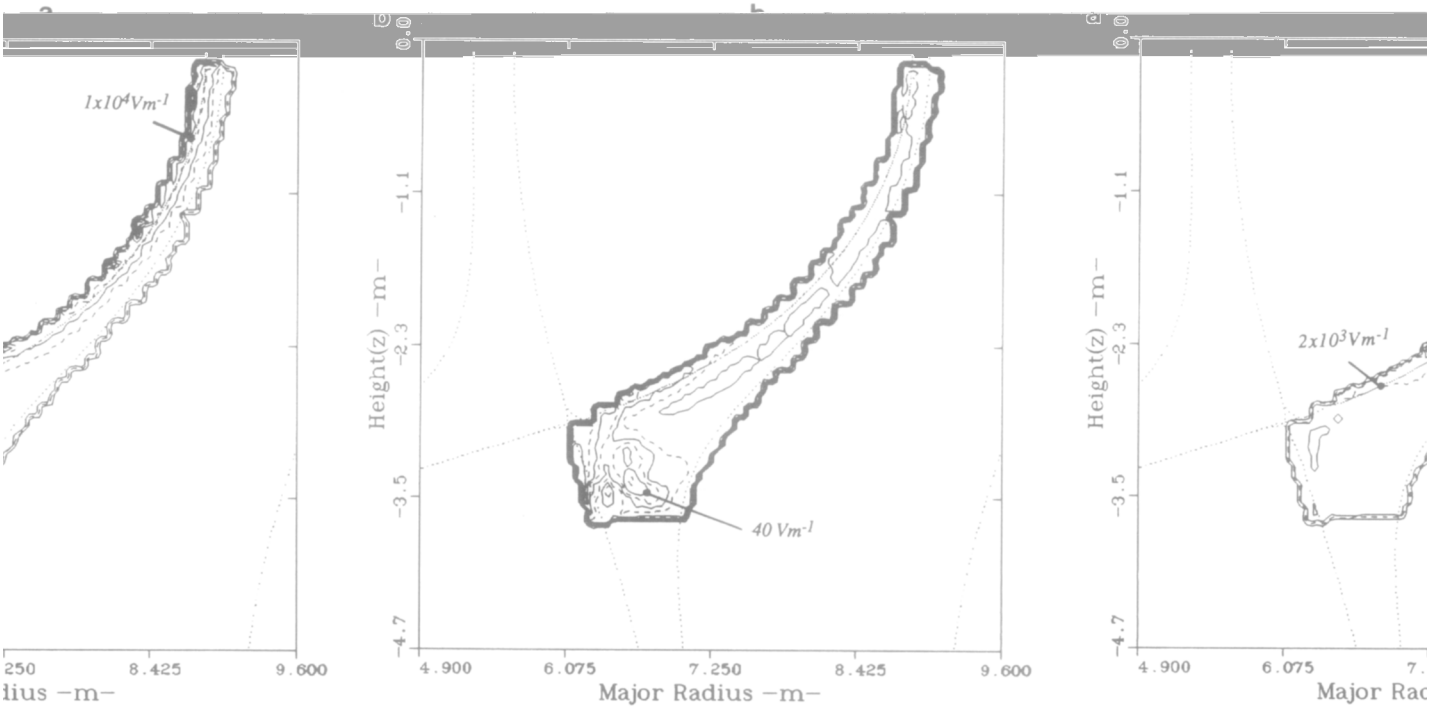

FIG. 11. (a) The plasma radial electric field exhibits steep radial and modest poloidal gradients with maximum values along the separatrix of 2×10^3 Vm^{-1} (midstream) to 1×10^4 Vm^{-1} (upstream). It is nearly zero at the outermost flux surface and throughout the divertor region. (b) The plasma poloidal electric field solution is in the range 25–40 Vm^{-1} in the divertor recycling region and near zero outside the divertor region.

edge plasma region has been implicated as a significant factor in global confinement both experimentally and theoretically [53]. The mechanism is not fully understood.

One suggestion to be pursued in a future computational study is that the combination of strong poloidal flows simultaneously with the strong poloidal and radial gradients in the electric field is sufficient to couple the mean and fluctuating flows, inducing turbulent transport in the plasma edge region. This can be examined in computational studies by introducing assumptions relating the fluctuating velocity to the mean flow in defining the momentum (and conductivity) tensors in the fluid equations, and then by solving the three coupled momentum equations consistently. A modest coupling between momentum components is expected to drive anomalously large cross-field flow because the parallel flow approaches sonic parameters. The examples show a high recycling solution, but the time dependent studies suggest that this solution may not be stable in the long term steady state operation. The complex flow patterns of plasma poloidal flux and poloidal gradient quantities suggests a turbulent edge plasma exists in this regime. More detailed studies will require distinguishing the electron and the ion responses to these complex plasma conditions.

The impact of the edge plasma on the core confinement is one of the most critical and least understood areas. This can be addressed realistically with a coupled edge-core plasma model [54], but work in this area is in its infancy and may be several years until a complete coupling. An ideal edge model would incorporate a core plasma transport model self-consistently to match the fluxes at the core-edge interface rather than specifying a boundary condition there. In ideal edge model would also require an MHD model to determine the magnetic flux surfaces evolving at each time step and prescribing the orthogonal grid on which the edge plasma fluid equations are solved.

The plasma edge is observed experimentally to be extremely complex. Considerable simplifying assumptions are needed to derive a fluid model to simulate the plasma and the neutral species in this region, leaving a gap between the dynamic plasma–neutral interactions and the relatively simple computational models. This computational effort is still in its infancy but is improving rapidly to model the edge plasma realistically.

VI. SUMMARY AND CONCLUSIONS

A 2D coupled plasma–neutral fluid computational model for the toroidally symmetric plasma edge region is presented. The neutrals are computed in a diffusion approximation implemented with a OGITE assumption. The plasma–neutral coupling allows a self-consistently computed numerical solution to problems related to "recycling" in the edge region. In its present form, the code does not address the problem of impurities which may play an important role in tokamak edge physics.

The plasma and neutral equations are finite discretized in a control volume approach which allows complex grids to conform with magnetic flux surfaces. A relaxation method for the time integration of the equations based on the SIMPLE method was found to be marginal for the compressible plasma with an inhomogeneous source term in the continuity equation. Improvement in performance was achieved by developing an "implicit diffusion" added to both sides of the continuity equation, allowing for time-dependent evolution. The steady state solution requires a large number of time steps, where the time step size is restricted by the advective plasma flows near the sonic plasma sheat boundary condition while the total time to steady state is determined by the particle recycling from the boundaries. This requires a residual correction to the continuity equation at each time step to assure a true convergence on the longer time scales associated with steady state.

The computational code has been calibrated in several studies that are detailed in separate reports [7, 23]. These studies find the present EPIC code results are realistic compared to other existing computational results and to experimental data from the tokamak program.

Some example output from the EPIC code is presented for a divertor tokamak operating at reactor relevant

ACKNOWLEDGMENTS

This work was performed at the Institute of Plasma and Fusion Research, University of California at Los Angeles, under a grant from the U.S. Department of Energy. The manuscript was completed at the Los Alamos National Laboratory operated by the University of California for the Department of Energy.

REFERENCES

1. D. E. Post and R. Behrisch, (Eds.), *Physics of Plasma Wall Interactions in Controlled Fusion* (Plenum, New York, 1986).
2. D. E. Post, "Role of Atomic Collisions in Fusion," in *Physics of Ion–Ion and Electron–Ion Collisions*, edited by F. Brouillard and J. W. McGowan (Plenum, New York, 1983), p. 37.
3. M. F. A. Harrison, "Boundary Plasmas," in *Applied Atomic Collision Physics*, Vol. I, edited by C. F. Barnett and M. F. A. Harrison, Ed. (Academic, New York, 1984), p. 395.
4. P. J. Harbour, *Nucl. Fusion* **24**, 1211 (1984).
5. D. E. Post and K. Lackner, in *Physics of Plasma Wall Interactions in Controlled Fusion*, edited by D. E. Post and R. Behrisch (Plenum, New York, 1986), p. 627.
6. M. F. A. Harrison, P. J. Harbour, and H. J. Hotston, *Nucl. Fusion/Tech.* **3**, 432 (1983).
7. E. L. Vold, Ph.D. dissertation, University of California at Los Angeles, 1989 (unpublished).

8. M. Sugihara, S. Saito, S. Hitoki, and N. Fujisawa, *J. Nucl. Mater.* **128/129**, 114 (1984).
9. H. Gerhauser and H. A. Claassen, *J. Nucl. Mater.* **176/177**, 721 (1990).
10. H. Gerhauser and H. A. Claassen, Report Jül-2125, KFA, Jülich, 1987 (unpublished).
11. B. J. Braams, in *11th European Conf. on Controlled Fusion and Plasma Physics, Aachen* **B34**, 431 (1983); see also B. Braams, in *12th European Conf. on Controlled Fusion and Plasma Physics, Budapest*, p. 480 (European physical Society, Petit-Lancy, Switzerland, 1985).
12. B. J. Braams, dissertation, The State University at Utrecht, The Netherlands, 1986 (unpublished).
13. R. Simonini, W. Feneberg, and A. Taroni, in *12th European Conf. on Controlled Fusion and Plasma Physics, Budapest*, p. 484 (European Physical Society, Petit-Lancy, Switzerland, 1985).
14. A. Nicolai and P. Borner, in *12th European Conf. on Controlled Fusion and Plasma Physics, Budapest*, p. 519 (European Physical Society, Petit-Lancy, Switzerland, 1985).
15. Yu. L. Igitkhanov, A. S. Kulcushkin, A. Yu. Pigarov, and V. I. Pistunovich, in *11th European Conf. on Controlled Fusion and Plasma Physics*, Aachen, A36, p. 397 (European Physical Society, Petit-Lancy, Switzerland, 1983).
16. M. Petravic, D. Heifetz, G. Kuo-Petravic, and D. Post, *J. Nucl. Mater.* **128/129**, 111 (1984).
17. S. Saito, T. Kobayashi, M. Sugihara, and N. Fujisawa, *J. Nucl. Mater.* **128/129**, 131 (1984).
18. N. Ueda, M. Kasai, M. Tanaka, M. Sugihara, and S. Sengoku, *Nucl. Fusion* **28**, 1183 (1988).
19. M. Petravic and G. Kuo-Petravic, *Nucl. Fusion* **30**, 1148 (1990).
20. D. Knoll and A. K. Prinja, *J. Nucl. Mater.* **176/177**, 562 (1990).
21. S. I. Braginskii, "Transport Processes in Plasmas," in *Reviews of Plasma Physics*, Vol. 1 (Consultants Bureau, New York, 1965).
22. F. L. Hinton and G. Staebler, in *12th International Conf. on Plasma Physics and Contr. Fusion Research, Nice, France*, Vol. II, p. 327 (IAEA, Vienna, 1988); see also Hinton and Staebler, *Nucl. Fusion* **29**(3), 405 (1989).
23. E. L. Vold, A. K. Prinja, F. Najmabadi, and R. W. Conn, *J. Nucl. Mater.* **176/177**, 570 (1990).
24. H. L. Stone, *SIAM J. Numer. Anal.* **5**, 530 (1968).
25. R. W. MacCormack, "Rapid Solver for Hyperbolic Systems of Equations," in *Proceedings, Fifth International Conf. on Numerical Methods in Fluid Dynamics* (Springer-Verlag, New York, 1976), p. 307.
26. E. L. Vold, F. Najmabadi, and R. W. Conn, *Phys. Fluids B* **3**(11), 3132 (1991).
27. J. F. Luciani, P. Mora, and J. Virmont, *Phys. Rev. Lett.* **51**, 1664 (1983).
28. P. Mora and J. F. Luciani, in *International Conf. on Plasma Phys., Kiev, USSR*, Vol. 2 (World Scientific Pub., Riveredge, NJ, 1987), p. 755.
29. J. J. Duderstadt and L. J. Hamilton, *Nuclear Reactor Analysis* (Wiley, New York, 1976).
30. M. Z. Hasan and R. W. Conn, *J. Comput. Phys.* **71**, 371 (1987).
31. W. J. Corbett, D. Reiter, R. W. Conn, K. H. Dipple, and K. H. Finken, *J. Vac. Sci. & Technol. A* **8**(3), 1772 (1990).
32. R. Chodura, in *Physics of Plasma-Wall Interactions in Controlled Fusion*, edited by D. E. Post and R. Behrisch (Plenum, New York, 1986), p. 99.
33. P. C. Stangeby, in *Physics of Plasma-Wall Interactions in Controlled Fusion*, edited by D. E. Post and R. Behrisch (Plenum, New York, 1986), p. 41.
34. R. C. Bissell, P. C. Johnson, and P. C. Stangeby, *Phys. Fluids B* **1**, 1133 (1989).
35. R. W. MacCormack, *SIAM-AMS Proc.* **11**, 130 (1978).
36. S. V. Patankar and D. B. Spalding, *J. Heat Mass Transfer* **15**, 1787 (1972).
37. S. V. Pantankar, *Numerical Heat Transfer and Fluid Flow* (Hemisphere, McGraw Hill, New York, 1981).
38. G. S. Deiwert, in *Proceedings, 4th Inter Conf. on Numerical Methods in Fluid Dynamics*, Lecture Notes in Physics, Vol. 35 (Springer-Verlag, New York, 1975), p. 132.
39. R. C. Grimm, J. M. Greene, and J. L. Johnson, *Methods Comput. Phys.* **9**, 253 (1976).
40. D. J. Strickler, J. D. Galambos, and Y-K. M. Peng, ORNL/FEDC-88/7, Oak Ridge National Laboratory, Oak Ridge, TN, 1989 (unpublished).
41. D. E. Potter and G. H. Tuttle, *J. Comput. Phys.* **13**, 483 (1973).
42. G. P. Maddison, Culham Lab. Report CLM-P-825, UKAEA, UK, 1987 (unpublished).
43. M. Petravic, *J. Comput. Phys.* **73**, 125 (1987).
44. F. H. Harlow and J. E. Welch, *Phys. Fluids* **8**, 2182 (1965).
45. E. S. Oran and J. P. Boris, *The Numerical Simulation of Reactive Flows* (Elsevier, New York, 1987).
46. D. A. Anderson, J. C. Tannehill, and R. H. Pletcher, *Computational Fluid Mechanics and Heat Transfer* (Hemisphere, New York, 1984).
47. P. J. Roache, *Computational Fluid Dynamics* (Hermosa, Albuquerque, NM, 1982).
48. D. S. Harned and W. Kerner, *J. Comput. Phys.* **60**, 62 (1985).
49. C. W. Hirt and F. H. Harlow, *J. Comput. Phys.* **2**, 114 (1967).
50. D. Heifetz, in *Physics of Plasma Wall Interactions in Controlled Fusion*, edited by D. E. Post and R. Behrisch (Plenum, New York, 1986), p. 695.
51. R. W. Conn, F. Najmabadi, and the ARIES Team, "ARIES I" paper IAEA-CN-53/H-1-4, in *13th International Conf. on Plasma Phys. and Contr. Nucl. Fusion Research, IAEA, Vienna, 1990*; see also ARIES I Report, Chap. 5, "Divertor Physics," Institute of Plasma and Fusion Research, UCLA, 1990 (unpublished).
52. C. D. Henning, "ITER in Perspective," *IEEE 13th Symposium on Fusion Energy, Knoxville, TN, 1989*, submitted; LLNL Report, UCRL-101756, Livermore, CA, 1989 (unpublished).
53. K. C. Shaing, *Phys. Fluids B* **2**, 764 (1990).
54. A. K. Prinja, R. Schafer, R. W. Conn, and H. Howe, *J. Nucl. Mater.* **145–147**, 868 (1987).